# The aging B cell landscape in atherosclerosis

Mol, J. de

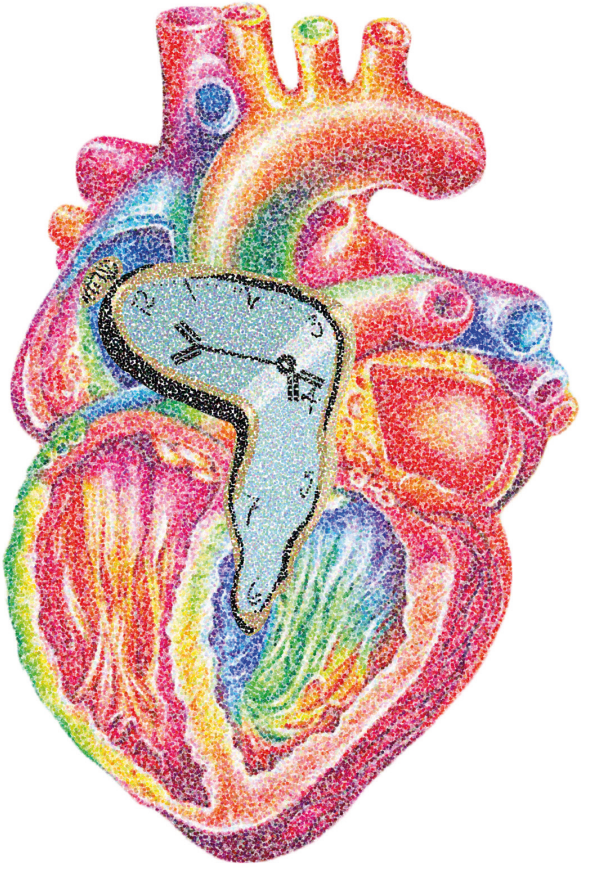

# Chapter 4

## Sexual dimorphism in atherosclerotic plaques of aged *Ldlr*$^{-/-}$ mice

*Immunity & Ageing, 2024 May 2; 21(1):27*

Virginia Smit[1], Jill de Mol[1], Mireia N.A. Bernabé Kleijn[1], Marie A.C. Depuydt[1], Menno P.J. de Winther[2], Ilze Bot[1], Johan Kuiper[1], and Amanda C. Foks[1]

1. Division of BioTherapeutics, Leiden Academic Centre for Drug Research, Leiden University, Einsteinweg 55, 2333 CC Leiden, The Netherlands
2. Amsterdam University Medical Centers – location AMC, University of Amsterdam, Experimental Vascular Biology, Department of Medical Biochemistry, Amsterdam Cardiovascular Sciences, Meibergdreef 9, 1105 AZ Amsterdam, The Netherlands.

# ABSTRACT

**Background**

Atherosclerosis, the main underlying pathology of cardiovascular disease, is a chronic inflammatory disease characterized by lipid accumulation and immune cell responses in the vascular wall, resulting in plaque formation. It is well-known that atherosclerosis prevalence and manifestation vary by sex. However, sexual dimorphism in the immune landscape of atherosclerotic plaques has up to date not been studied at high resolution. In this study, we investigated sex-specific differences in atherosclerosis development and the immunological landscape of aortas at single-cell level in aged *Ldlr*$^{-/-}$ mice.

**Methods**

We compared plaque morphology between aged male and female chow diet-fed *Ldlr*$^{-/-}$ mice (22 months old) with histological analysis. Using single-cell RNA-sequencing and flow cytometry on CD45$^{+}$ immune cells from aortas of aged *Ldlr*$^{-/-}$ mice, we explored the immune landscape in the atherosclerotic environment in males and females.

**Results**

We show that plaque volume is comparable in aged male and female mice, and that plaques in aged female mice contain more collagen and cholesterol crystals, but less necrotic core and macrophage content compared to males. We reveal increased immune cell infiltration in female aortas and found that expression of pro-atherogenic markers and inflammatory signaling pathways was enriched in plaque immune cells of female mice. Particularly, female aortas show enhanced activation of B cells (*Egr1*, *Cd83*, *Cd180*), including age-associated B cells, in addition to an increased M1/M2 macrophage ratio, where *Il1b*$^{+}$ M1-like macrophages display a more pro-inflammatory phenotype (*Nlrp3*, *Cxcl2*, *Mmp9*) compared to males. In contrast, increased numbers of age-associated Gzmk$^{+}$CD8$^{+}$ T cells, dendritic cells, and *Trem2*$^{+}$ macrophages were observed in male aortas.

**Conclusions**

Altogether, our findings highlight that sex is a variable that contributes to immunological differences in the atherosclerotic plaque environment in mice and provide valuable insights for further preclinical studies into the impact of sex on the pathophysiology of atherosclerosis.


**Keywords:** cardiovascular disease, atherosclerosis, aging, sex, immunology, single-cell transcriptomics

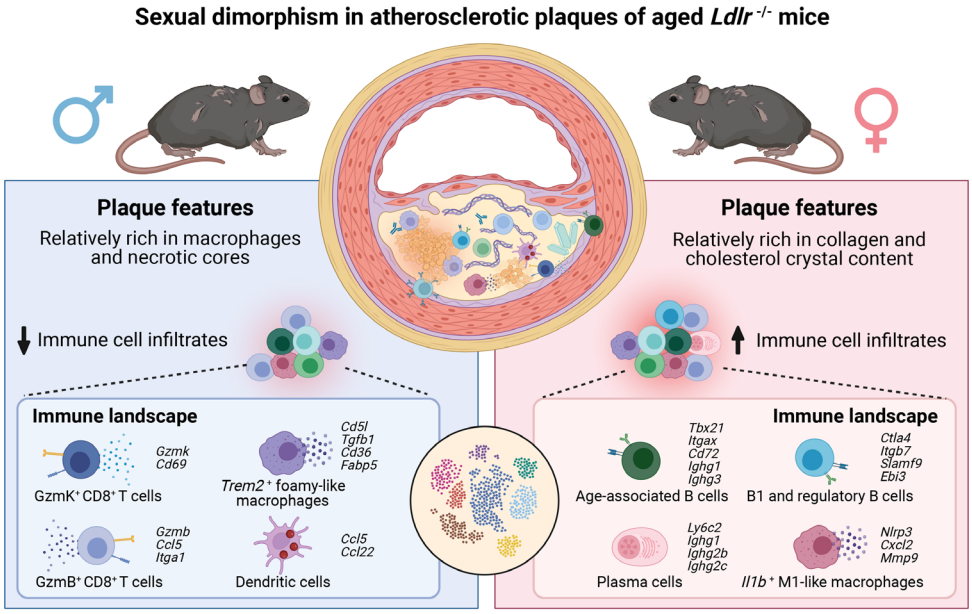


**Graphical abstract.**

# INTRODUCTION

Atherosclerosis, a chronic inflammatory disease characterized by lipid accumulation and immune cell infiltration in the arterial wall, is the main underlying pathology of cardiovascular disease (CVD). Although CVD is the leading cause of death in both women and men, accounting for 45% and 39% of all deaths respectively[1,2], sex differences in atherosclerotic CVD prevalence and manifestation have been described. CVD develops about 10 years later in women than in men[3] but women have a poorer prognosis and are more likely to die following an acute cardiovascular event.[4] While acute cardiovascular events in women are mostly caused by stable atherosclerotic plaques that undergo erosion, in men, acute plaque rupture is often the culprit factor.[5] Moreover, women generally have smaller plaque area with decreased necrotic core volume compared to men.[6,7] Incidence of thin-cap fibroatheroma and large calcification area varies by sex, but only when stratified by age, since men younger than 70 years of age showed a higher prevalence of thin-cap fibroatheroma and large calcification , while women older than 70 years showed a higher prevalence.[8] Notably, CVD risk in women is often missed due to the assumption that women are "protected" against CVD at younger age. Combined with the underrepresentation of women in scientific research, these factors contribute to a knowledge gap regarding the pathophysiology of atherosclerotic CVD in women.[9]

Inflammation of the arterial wall is a key driver of atherosclerosis pathogenesis. Evidently, human and mouse studies that mapped the immune landscape of atherosclerotic plaques with single-cell technologies showed a heterogenous leukocyte pool within the plaque, including innate and adaptive immune cells.[10–14] Lymphoid cells, particularly T cells, were highly abundant in human atherosclerotic plaques and plaques of aged *Ldlr*$^{-/-}$ mice.[15] However, sexual dimorphism in the immune landscape of atherosclerotic plaques is seldomly studied. At a transcriptomic level, Hartman and colleagues reported significant sex-specific differences in sex-stratified gene regulatory networks from bulk RNA-sequencing derived from atherosclerotic aortic root tissue.[16] Genes that were more active in women were associated with mesenchymal and endothelial cells, while genes more active in men were associated with the immune system, particularly macrophages. Detailed profiling of plaque-residing immune cells is however lacking. Moreover, only few preclinical studies compared plaque immune cell numbers in the aortic root or arch between sexes, where either no differences were found either between sexes or increased infiltration of T cells in male chow diet-fed *Apoe*$^{-/-}$ mice.[17–20] None of them have taken aging into account, one of the most dominant risk factors of CVD.[21]

To bridge this knowledge gap, we investigated sex-specific differences in the atherosclerotic plaque of aged *Ldlr*$^{-/-}$ mice, a highly translational preclinical atherosclerosis model.[15] We compared plaque morphology between males and females with histological analysis. Using single-cell RNA-sequencing and flow cytometry on CD45$^{+}$ immune cells from aortas of aged *Ldlr*$^{-/-}$ mice, we explored the immune landscape in the atherosclerotic environment in males and females.

# MATERIALS & METHODS

**Animals**

All animal experiments were approved by the Leiden University Animal Ethics Committee and were performed according to the guidelines of the European Parliament Directive 2010/63/EU of the European Parliament. Male and female *Ldlr*$^{-/-}$ mice on a C57Bl/6J genetic background (3 months or 20 months old at the start of the experiment) were bred and aged in-house and kept under standard laboratory conditions. Young (3 months old) mice were randomized according to weight and basal serum cholesterol levels, and fed a regular chow diet (CD) or a Western diet (WD) containing 0.25% cholesterol and 15% cocoa butter (Special Diet Services, Witham, Essex, UK) for 10 weeks. Diet and water were provided *ad libitum*. At the end of experiment, mice were anaesthetized by a subcutaneous injection of a cocktail containing ketamine (100 mg/kg), atropine (0.5 mg/kg), and xylazine (10 mg/kg). Mice were bled by retro-orbital bleeding, and tissues were harvested after *in situ* perfusion with phosphate buffered saline (PBS). One mouse was excluded from the experiment due to presence of tumors.



**Histology**

Hearts and aortas were embedded in O.C.T. compound (Sakura) and snap-frozen. To determine lesion size, cryosections (10 µm) of the aortic root were stained with Oil-Red-O and hematoxylin (Sigma-Aldrich). To quantify lesion volume, sections were collected from when aortic valves started to appear until a distance of 1.2 mm relative to the root was reached. The average of five sequential sections of the three-valve area of aortic roots, displaying the highest lesion content, was used to compare the vessel occlusion. Collagen content in the lesions was quantified using a Masson's trichrome staining (Sigma-Aldrich). The necrotic core was defined as the acellular, debris-rich lesion area as percentage of total plaque area. Corresponding sections on separate slides were stained for monocyte/macrophage content with a MOMA-2 antibody (1:1000, AbD Serotec) followed by a biotinylated goat anti-rat IgG antibody (1:200, Vector). Secondary antibodies were detected using the Vectastain ABC kit (Vector) and visualized with ImmPACT NovaRED HRP substrate (Vector). We categorized cholesterol crystallization of atherosclerotic lesions in the aortic root on a scale of 0 (no cholesterol crystallization) to 3 (>75% of the lesion area contains crystalline cholesterol). Presence of calcification was manually scored based on morphology. To quantify calcification area, sharp demarcated acellular dark pink to purple areas in the hematoxylin staining of three consecutive sections were divided by total plaque area.[22] Analysis and scoring were performed blinded. Mice with bicuspid aortic valves were excluded from histological analyses (n=3). Pictures were taken with a Mikrocam II (Besser) linked to a Leica DM6000 Microscope. Stained sections were manually analyzed with ImageJ software.

**Aortic CD45$^{+}$ cell isolation for single-cell RNA-sequencing**

Atherosclerotic aortic arches, carefully detached from other surrounding organs, extensively flushed with PBS, and thoroughly cleaned from any residual perivascular adipose tissue , were isolated from aged chow diet-fed male *Ldlr*$^{-/-}$ mice (22 months old; n=23) and enzymatically digested as previously described.[15] Single-cell suspensions were stained with Fixable Viability Dye eFluor™ 780 (1:2000, eBioscience) and CD45-PE (1:500, clone 30-F11, Biolegend). After removing doublets, alive CD45$^{+}$

cells were sorted (**Supplementary Figure 1**) using a 100µm nozzle in PBS supplemented with 0.04% BSA using a FACS Aria II SORP (BD Biosciences) and immediately processed for single-cell RNA-sequencing (scRNA-seq).

**Single-cell library preparation**

Aortic CD45$^+$ cell suspensions were loaded on a Chromium Single Cell instrument (10x Genomics) to generate single cell gel bead emulsions (GEMs). ScRNA-seq libraries were prepared using the Single Cell 3' Solution v2 Reagent Kit (10xGenomics). Sequencing was performed on an Illumina HiSeq2500 and the digital expression matrix was generated by de-multiplexing barcode processing and gene UMI (unique molecular index) counting using the Cell Ranger v6.0 pipeline (10x Genomics).

**Single-cell data processing, integration, and analysis**

The digital expression matrix of aortas isolated from chow diet-fed aged male *Ldlr*$^{-/-}$ mice and of the female *Ldlr*$^{-/-}$ mice, that was recently published[15], were analyzed using the R package Seurat (version 4). Cells were filtered by unique gene count per cell >200 and <6,000 for aged male, and >200 and <7500 for aged female. In addition, a cutoff was set to a maximum of 6%, and 12% mitochondrial gene expression for aged male and aged female samples, respectively. Doublets were identified and removed using the DoubletDecon package. The remaining 5294 (aged male) and 4674 (aged female) cells were log-normalized, integrated using canonical correlation analysis and scaled subjected to principal component analysis (PCA). Based on the elbow plot, Jackstraw functions and separation of marker genes, 16 PCA components were included for cluster detection at a resolution of 0.245, which were subsequently visualized through Uniform Manifold Approximation and Projection (UMAP).

The Seurat function FindAllMarkers was used to find the differentially expressed genes (DEGs) per cluster, which were examined to define the cell clusters. For the high-resolution re-clustering, (*Cd79b*$^+$) B cell clusters, (*Cd3e*$^+$) T cell clusters and (*Cd68*$^+$ and *Itgam*$^+$) myeloid clusters were selected and extracted from the main clustering. Thresholds were set to *Cd19*<0.3, *Cd79b*<0.3, *Cd68*<0.3 to exclude non-T cells from the T cell clustering, *Cd3e*<0.3, *Cd68*<0.3 to exclude non-B cells from the B cell clustering, and *Cd3e*<0.3, *Cd19*<0.3, *Cd79b*<0.3 to exclude non-myeloid cells from the myeloid clustering. The variable genes of these selected clusters were then used as input for dimensionality reduction and re-clustering. PCA analysis on rescaled transcripts was performed with the following dimensions and resolutions: T cells (3155 cells), dimensions 9, resolution 0.6; B cells (2746 cells), dimensions 11, resolution 0.25; myeloid cells (1818 cells), dimensions 12, resolution 0.5. Tregs (*Foxp3*>0.3) and non-Tregs (*Foxp3*<0.3) were selected from cluster 4 CD4$^+$ T cells (*Cd8a*<0.3, *Cd8b1*<0.3, *Tcrg-C1*<0.3, *Cd4*>0.4, *Kit*<0.3). UMAP plots, dot plots, violin plots, volcano plots were generated in R. Enrichment scores of the SenMayo geneset were calculated using the AUCell package.[23,24] Pathway analyses were performed using the Single Cell Pathway Analysis (SCPA) package.[25]

**Flow cytometry**

Immunostaining was performed as previously described on single cell suspensions derived from murine aortas to characterize immune cells.[15] To block Fc receptors, an unconjugated anti-CD16/32 antibody (clone 2.4G2, BD Bioscience) was used for mouse samples. Living cells were selected using Fixable

Viability Dye eFluor™ 780 (1:2000, eBioscience) and different cell populations were defined using anti-mouse fluorochrome-conjugated antibodies (**Supplementary Table S1**). Antibody staining of transcription factors and cytokines was performed using transcription factor fixation/permeabilization concentrate and diluent solutions and cytofix/permeabilization solutions, respectively (BD Biosciences). Flow cytometry analysis was performed on a Cytoflex S (Beckman Coulter) and the acquired data were analyzed using FlowJo software (version 10.7).

### Statistical analysis

Data are expressed as mean ± SEM. Outliers were identified and removed using Grubbs outlier tests (α= 0.05). Significance of data with more than 2 groups was tested using one-way ANOVA test followed by a Tukey multiple comparisons test. Statistical significance of data with 2 groups was tested using an unpaired two-tailed t-test or a nonparametric Mann-Whitney U test. Plotted comparisons are between males and females per age group. P-values of <0.05 were considered significant. Statistical analysis was performed using GraphPad Prism 9.0.

## RESULTS



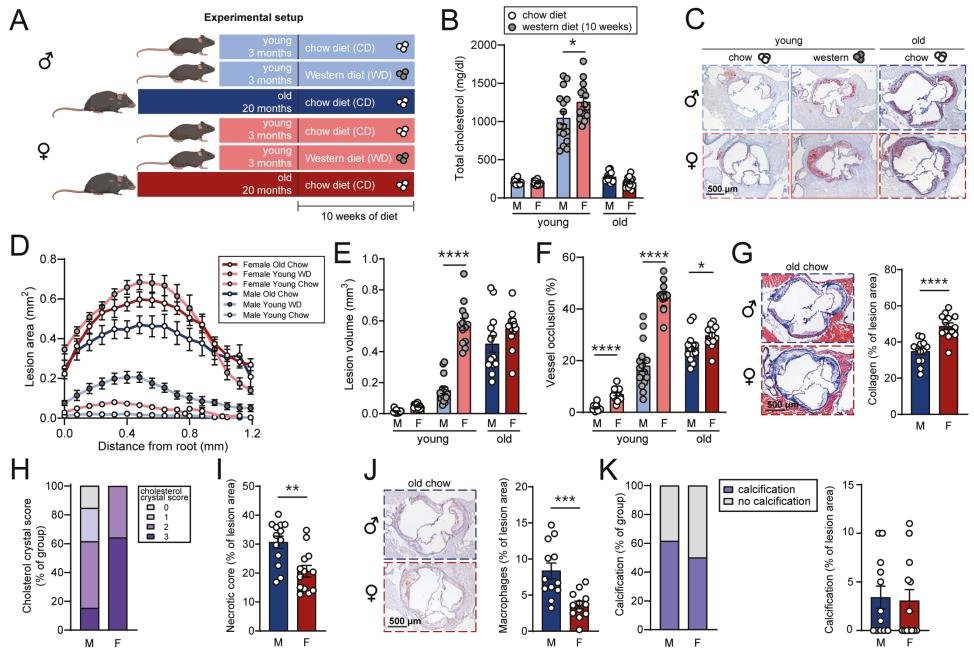


**Figure 1. Plaque size and composition of aged male and female *Ldlr*$^{-/-}$ mice. A)** Experimental setup: young male (light blue) and young female[15] (light red) *Ldlr*$^{-/-}$ mice were randomized according to weight and basal serum cholesterol levels and fed a chow diet (white circles) or western diet (grey circles) for 10 weeks, and old male (dark blue) and old female[15] (dark red) *Ldlr*$^{-/-}$ were fed a chow diet. **B)** Total serum cholesterol levels at sacrifice were measured. **C)** Cross sections of the aortic root were stained for lipid and collagen content. **D)** Atherosclerotic lesion area over distance, **E)** lesion volume, and **F)** vessel occlusion were quantified. **G)** Collagen content was quantified as percentage of lesion area. **H)** Cholesterol crystallization in atherosclerotic lesions was categorized on a scale of 0 (no cholesterol crystallization) to 3. **I)** Necrotic cores and **J)** macrophage content (MOMA-2) were measured as percentage of lesion area. **K)** Presence of calcification (purple) or no calcification (grey) was presented as percentage of the group and measured as percentage of lesion area. Data are from n = 12–16 mice per group. Statistical significance was tested by one-way ANOVA. Mean ± S.E.M. plotted. *P < 0.05, **P < 0.01, ***P < 0.001, ****P < 0.0001.

**Atherosclerotic lesions of aged female mice are rich in collagen and cholesterol crystals**

The *Ldlr*$^{-/-}$ mouse is a widely used experimental model to study atherosclerosis, but we and others have previously shown that severe hypercholesterolemia induced by a Western diet (WD) is needed to promote atherosclerosis in young (3 months) *Ldlr*$^{-/-}$ mice (**Figure 1A-D**).[15] Notably, as shown in **Figure 1D-E**, young female *Ldlr*$^{-/-}$ mice are more prone to develop atherosclerosis compared to young male *Ldlr*$^{-/-}$ mice upon WD feeding. However, this WD-accelerated induction of atherosclerosis in young mice diverges from the gradual buildup of atherosclerotic lesions and pathology that comes with aging as manifested in humans. We therefore investigated sex-related differences in atherosclerotic plaque development, composition, and the immune landscape in a more translational setting, using chow diet (CD)-fed aged (22 months) *Ldlr*$^{-/-}$ mice (~200-250 mg/dl serum cholesterol, **Figure 1B**) of both sexes. As opposed to the large discrepancy of lesion volume between sexes in the young WD-fed mice, lesion volume between aged male and female CD-fed mice did not statistically differ, although vessel occlusion was still slightly elevated in aged CD-fed females (**Figure 1E-F**). Atherosclerotic lesions of aged female *Ldlr*$^{-/-}$ mice were relatively enriched in collagen content and cholesterol crystals but showed less necrotic core and macrophage content compared to male mice (**Figure 1I-J**). Calcification incidence and content, which significantly increases in aged atherosclerotic mice[15], were comparable between both sexes (**Figure 1K**).

**Single-cell profiling reveals increased immune cell infiltration in the aorta of aged female mice**

Next, we sought out to explore sex differences in the immunological landscape of the aged atherosclerotic plaque and identify unique and conserved gene expression signatures of distinct plaque immune cell types between aged male and female mice. We performed single-cell RNA sequencing analysis on CD45$^{+}$ cells obtained from the atherosclerotic aortic arch of aged female *Ldlr*$^{-/-}$ mice[15], and integrated this with scRNA-seq data of aged male *Ldlr*$^{-/-}$ mice (**Figure 2A**). To identify distinct immune cell types in the atherosclerotic plaque of males and females, we performed dimensionality reduction and unsupervised cell clustering on a total of 9968 cells (male: 5294 cells, and female: 4674 cells). We observed overlapping alignment of the male and female immune cell clusters (**Figure 2B**), indicating proper batch effect correction and consistency in cluster definition across sexes. Immune cell clusters were defined by canonical marker genes and visualized in a UMAP plot and proportional abundance barplot (**Figure 2C-D** and **Supplementary Figure S2A-C** and **Table S2**). Proportionally, we observed increased abundance of CD8$^{+}$ T cells in male aortas, while populations of CD4$^{+}$CD8$^{+}$ double positive (DP) T cells, CD21$^{-}$CD23$^{-}$ B cells and *Il1b*$^{+}$ macrophages (MF) were increased in female aortas (**Figure 2D**). We also measured sex-specific changes in major immune cell abundance with flow cytometry and found increased immune cell infiltration in the aortic arches of female mice (**Figure 2E**). In agreement with the scRNA-seq data, male aortic arches showed increased numbers of CD8$^{+}$ T cells and myeloid cells, whereas female aortic arches contained more CD19$^{+}$ B cells and CD4$^{+}$CD8$^{+}$ DP T cells (**Figure 2E** and **Supplementary Figure S2D** and **S3**).

To investigate potential sex-specific differences of senescence in the aortic leukocytes of these aged mice, we performed enrichment of the SenMayo senescence gene set.[23] Although B and T cells did not show any sex-specific difference, NK cells and to a lesser extent myeloid cells of female aortas displayed enrichment of senescence (**Figure 2F**). In line with this, we observed increased expression

of senescence-associated secretory phenotype (SASP) genes (e.g. chemokines, *Mmp9*, *Il1b*, *Tnf*), intracellular (e.g. *Gem*, *Icam1*, *Jun*) and transmembrane senescence-associated genes (e.g. *Cxcr2*, and STAT3 target genes *Tnfrsf1a/b*) in NK cells and myeloid cells of females (**Figure 2G**). To gain further insight into possible sex differences within the subsets, we next performed reclustering of each major immune cell population (B cells, T cells and myeloid cells).

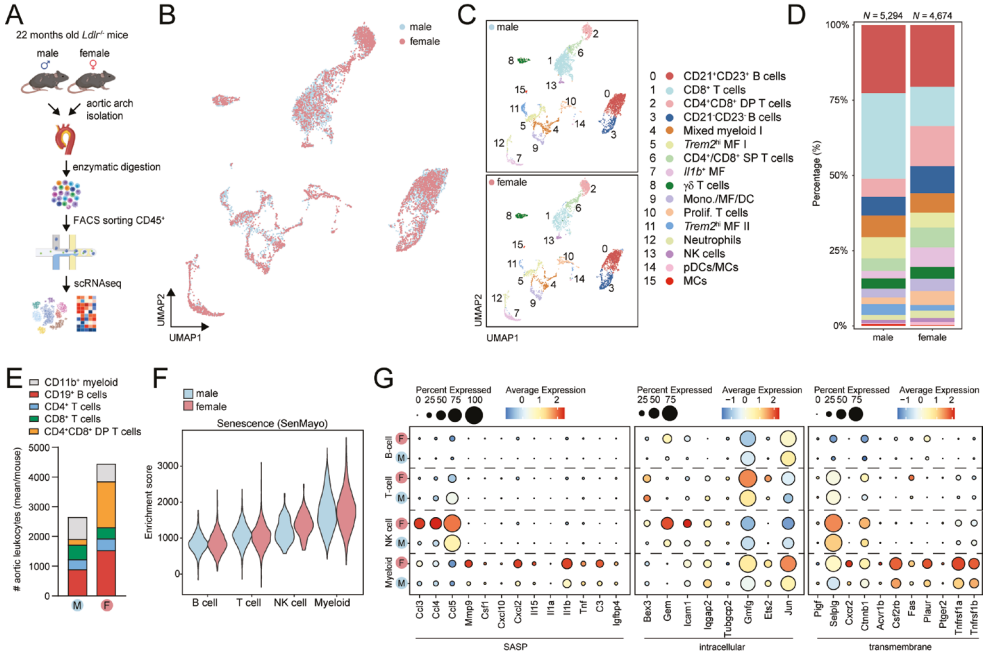


**Figure 2. Immune cell landscape of aortas from aged male and female *Ldlr*$^{-/-}$ mice. A)** Workflow of scRNA-seq on aortic CD45$^{+}$ cells of chow diet-fed 20-months-old male (n = 23) and female (n = 12) *Ldlr*$^{-/-}$ mice. UMAP visualization of clustered aortic leucocytes grouped by **B)** sex or **C)** immune cell clusters. **D)** Stacked diagram showing the relative proportions of major immune cell subtypes within CD45$^{+}$ cells of *Ldlr*$^{-/-}$ aortas measured by scRNA-seq. **E)** Stacked diagram showing the number of major immune cell types in the aorta of aged male and female *Ldlr*$^{-/-}$, measured as mean per mouse with flow cytometry. **F)** Violin plot showing the senescence (SenMayo gene set) enrichment score of major immune cell types per sex. **G)** Average expression of SASP, intracellular and transmembrane genes from the SenMayo gene set in major immune cell types split by sex. DP, double positive; MF, macrophages; SP, single positive; DC, dendritic cell; NK, natural killer; pDC, plasmacytoid dendritic cell; MC, mast cell.

### Activated age-associated B cells are enriched in aortas of female mice

Proportionally, B2-like cells (cluster 0; *Ighd*, *Fcer2a*, *Cr2*) comprised the largest B cell cluster in aortas of both sexes (males 66% and females 54%) (**Figure 3A**, **Supplementary Figure S4 and B**, and **Supplementary Table S3**). We further detected B1-like cells and regulatory B cells (cluster 1; *Zbtb32*, *S100a6*, *Cd9*), age-associated B cells (ABCs, cluster 2; *Zbtb20*, *Tbx21*, *Fas*), Ifn-induced B cells (cluster 3; *Ifit2*, *Ifit3*, *Ifi213*), activated B cells enriched for Myc-target genes (cluster 4; *Nme2*, *Mif*), immature B cells (cluster 5; *Cd93*, *Cd24a*), plasma cells (cluster 6; *Sdc1*, *Jchain*, *Prdm1*) and undefined B cells (cluster 7).

Not surprisingly, DEG analysis showed upregulation of X-chromosomal genes (*Xist*, *Tsix*, *Gm6377*) in female B cells, while Y-chromosomal genes *Eif2s3y* and *Ddx3y* were upregulated in male B cells (**Figure 3B**). Female B cells displayed upregulation of activation-related genes *Cd40*, *Cd80*,

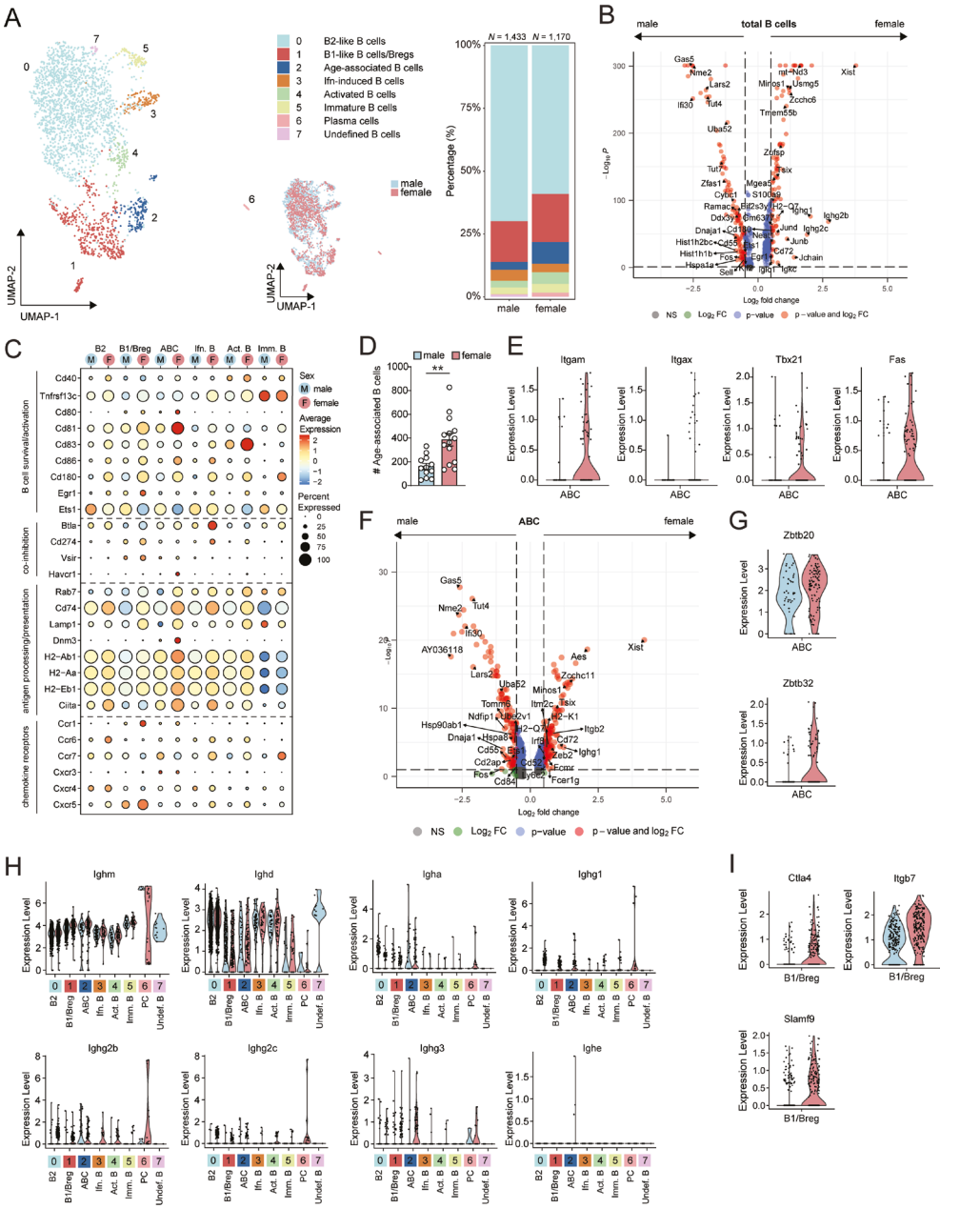


**Figure 3. Sex-specific gene signatures of aortic B cells in aged *Ldlr*$^{-/-}$ mice. A)** UMAP plots and stacked diagram of B cell clusters in the aorta of *Ldlr*$^{-/-}$ mice. **B)** Volcano plot displaying differentially expressed genes of the total B cell subclustering between aged male and female *Ldlr*$^{-/-}$ mice. **C)** Average expression of biological process-associated genes in B cell clusters split by sex. **D)** Absolute number of age-associated B cells in the aortas of aged male and female *Ldlr*$^{-/-}$ mice was measured with flow cytometry. **E)** Sex-specific gene expression level of age-associated B cell-specific markers in cluster 2. **F)** Volcano plot of cluster 2 displaying differentially expressed genes between male and female. Sex-specific expression level of **G)** zinc-finger protein genes in cluster 2, **H)** immunoglobulin isotype genes in all B cell clusters, and **I)** genes differentially expressed in cluster 1. Flow cytometry data are from n = 12–14 mice per group. Statistical significance was tested by a t-test. Mean ± S.E.M. plotted. $^{**}P < 0.01$.

*Cd83*, *Cd86*, *Egr1*, *Cd180*[26–30], while B cells in male aortas exhibited high expression of *Ets1*, a transcription factor that negatively controls B cell activation and concomitant antibody-secreting cell function[31], suggesting that B cells in males are less likely to contribute to humoral immunity (**Figure 3B** and **C**). Additionally, expression of genes encoding co-inhibitory molecules was relatively higher in females compared to males, where *Havcr1* expression (Tim-1) was particularly high in the ABC cluster. Although hard to detect, both pro- and anti-inflammatory cytokine genes were mostly expressed at higher levels in female B cells (**Supplementary Figure S4C**). A similar pattern was seen in antigen-processing and presentation-related genes, particularly in ABCs. Strikingly, ABCs were more abundant in atherosclerotic aortic arches of aged female than in aged male *Ldlr*$^{-/-}$ mice, which was confirmed with flow cytometry (386±53 vs. 161±26 cell count, P<0.01; **Figure 3A** and **3D**). ABCs in females showed high expression levels of ABC-characteristic marker genes *Tbx21* (T-bet), *Fas*, and particularly *Itgax* (CD11c; **Figure 3E**). Also, *Itgb2* (encoding CD18 that forms the functional CR4 complex with CD11c) and *Cd72* (encoding a transmembrane molecule that can regulate B cell activation) were upregulated in female ABCs (**Figure 3F**).[32,33] *Cxcr3*, a chemokine receptor that is likely to be involved in the migration of B cells to the site of inflammation and differentiation into antibody-secreting plasma cells[34,35], is almost exclusively expressed by the ABC cluster, but expression levels were comparable between sexes (**Figure 3C**).



Certain zinc finger genes (*Zbtb20*, *Zbtb32*) in B cells are associated with plasma cell differentiation[36,37], and expression levels of these genes were elevated in female ABCs (**Figure 3G**). In line with this, plasma cells characterized by high expression of immunoglobulin-encoding genes and *Ly6c2*[38], were more abundantly present in female aortas (**Figure 3A**, **H** and **Supplementary Figure S4D**). Overall, immunoglobulin-encoding genes were more expressed in B cell clusters of females, of which ABCs showed high expression of *Ighg1* and *Ighg3* compared to other B cell clusters (excluding plasma cells; **Figure 3H**). Notably, gene expression of *Ctla4* (co-inhibitory molecule), *Slamf9* (upregulated by inflammatory stimulus on B1 cells) and *Itgb7* (involved in homing of B cells) was increased in the female B1/Breg cluster[39–41], suggesting a more inflammatory and activated profile of the B1/Breg cluster in female mice (**Figure 3I**).

**Granzyme-expressing effector CD8+ T cells are enriched in atherosclerotic aortas of aged males**

The aortic T cell pool of aged *Ldlr*$^{-/-}$ mice contained 3 CD8$^+$ T cell clusters, specifically *Gzmk*$^+$CD8$^+$ T cells (cluster 0; *Gzmk*, *Nkg7*, *Eomes*), *Gzmb*$^+$CD8+ T cells (cluster 2; *Gzmb*, *Klrk1*, *Ly6c2*), and *Sell*$^+$CD8$^+$ T cells (cluster 3; *Sell*, *Klf2*, *Foxp1*; **Figure 4A** and **Supplementary Figure S5A** and **B** and **Table S4**). CD8$^+$ T cells comprised 63.3% of aortic T cells in males compared to 28.3% of aortic T cells in females (**Figure 4A**). While CD4$^+$CD8$^+$ double positive (DP) T cells (cluster 1; *Rag1*, *Arpp21*, *Ccr9*) were the largest T cell cluster in the female aortic arches, the proportion of CD4$^+$ T cells (cluster 4; *Tnfrsf4*, *Izumo1r*, *Icos*) did not differ between the sexes. These sex-specific frequencies of main T cell populations were also confirmed with flow cytometry (**Figure 4B**). Additionally, we identified proliferating T cells (cluster 5; *Mki67*, *Pclaf*, *Nusap1*), *Tox*$^{hi}$ T cells (cluster 6; *Tox*, *Itm2a*, *Nab2*), γδ T cells (cluster 7; *Tcrg-C1*, *Serpinb1a*, *Tmem176a/b*) and a cluster of mixed cells (cluster 8; *Malat1*, *Lck*).

Analysis on total T cells showed that compared to females, the male T cell compartment was enriched

in the natural killer pathway and cytotoxic/effector-related genes (*Nkg7*, *Ccl5*, *Klrd1*, *Gzmb*, *Gzmk*) and (**Figure 4C-D**). In contrast, CTLA-4, TCR and interleukin-related pathways (red dots in **Figure 4C**) were more enriched in female T cells. Moreover, effector molecules (*Prf1*, *Ccl4*) and cytokines (*Ifng*, *Tnf*, *Il2*, *Tgfb1*) were expressed at higher levels in T cells from females than from males, particularly in the *Gzmb*$^{+}$CD8$^{+}$ T cells (**Figure 4E**). *Gzmk*$^{+}$CD8$^{+}$ T cells were more abundant in males, as measured by scRNA-seq as well as with flow cytometry (**Figure 4A** and **F**) and showed comparable gene expression of effector molecules and cytokines, but increased expression of some exhaustion markers (*Lag3*, *Ctla4*) in females (**Figure 4E**). In addition, *Ccl5* and the gene encoding its receptor *Ccr5* were expressed on the majority of the *Gzmb*$^{+}$ and *Gzmk*$^{+}$CD8$^{+}$ T cells. Interestingly, genes associated with T cell migration (*Itga1*, *Itga4*) and activation marker *Cd69* were expressed at higher levels in both granzyme-expressing CD8$^{+}$ T cell clusters of males compared to females.

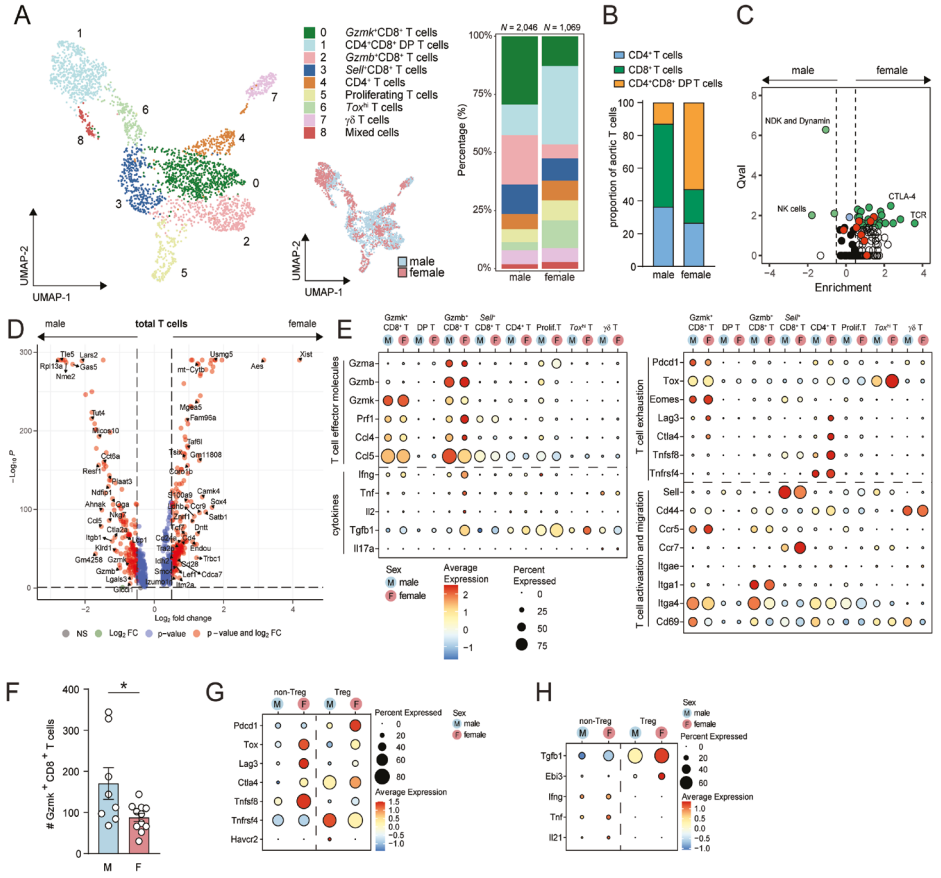


**Figure 4. Transcriptomic comparison of T cells in aortas of aged male and female *Ldlr*$^{-/-}$ mice. A)** UMAP plots and stacked diagram of T cell clusters in the aorta of *Ldlr*$^{-/-}$ mice. **B)** Stacked diagram showing the relative proportions of CD4$^{+}$, CD8$^{+}$ and CD4$^{+}$CD8$^{+}$ T cells within aged male and female *Ldlr*$^{-/-}$ aortas, measured by flow cytometry. **C)** Pathway enrichment of T cells in male and female mice. Green dots: significantly enriched pathways; red dots: interleukin-related pathways; white dots: insignificantly enriched pathways; black dots: insignificantly unenriched pathways. **D)** Volcano plot displaying differentially expressed genes of the total T cell subclustering between aged male and female *Ldlr*$^{-/-}$ mice. **E)** Dot plot displaying the sex-specific expression of biological process-associated genes in T cell clusters. **F)** Absolute number of Gzmk$^{+}$CD8$^{+}$ T cells in the aortas of aged male and female *Ldlr*$^{-/-}$ mice was measured with flow cytometry. Average gene expression of **G)** costimulatory and coinhibitory molecules and **H)** cytokines in Tregs and non-Tregs from CD4$^{+}$ T cells in cluster 4, split by sex.

Cluster 4 mainly consisted of CD4$^+$ T cells, including regulatory *Foxp3*$^+$CD4$^+$ T cells (Treg), but also contained some remainder *Kit*$^+$ mast cells (**Supplementary Figure S5B**). In female atherosclerotic aortic arches, this cluster was enriched for *Lag3*, *Ctla4*, *Tnfsf8* (CD30L; **Figure 4E**). Upon division of cells from cluster 4 into *Foxp3*$^+$CD4$^+$ Tregs and *Foxp3*$^-$CD4$^+$ non-Tregs, we found that Tregs in females showed higher expression of *Pdcd1* (PD-1), *Ctla4* and *Tnfrsf4* (OX40) but lower expression of *Havcr2* (TIM-3), while non-Treg CD4$^+$ T cells in females specifically showed higher expression of *Tox*, *Lag3*, and *Tnfsf8* (**Figure 4G**). This may indicate increased presence of the recently described CD30L$^+$PD-1$^+$CD44$^+$CD4$^+$ senescence-associated T cells[42] in aged aortas of female compared to male mice (**Supplementary Figure S5C**). Additionally, Tregs in females displayed higher expression of anti-inflammatory cytokine genes *Tgfb1* and *Ebi3* (IL-35), whereas non-Tregs in females showed elevated expression levels of *Tnf*, *Il18*, and *Il21* compared to non-Tregs in males (**Figure 4H**).

**Female bias towards inflammatory M1-like macrophages in the aorta**

The aortic myeloid cell compartment contained M1- and M2-like macrophages, resident macrophages, dendritic cells, monocytes, neutrophils, and mast cells (**Figure 5A** and **Supplementary Figure 6A** and **B**). DEG analysis showed upregulation of *Cxcl2*, *Il1b* and *Ccl3* in aortic myeloid cells of *Ldlr*$^{-/-}$ females, while *Fabp5*, *Apoe*, *Cd5l* and *Spp1* were upregulated in myeloid cells from *Ldlr*$^{-/-}$ males (**Figure 5B**). *Il1b*$^+$ M1-like macrophages (*Il1b*, *Csf3r*, *Cxcr2*) were the most abundant myeloid population in females (~30% in females vs. ~10% in males). Moreover, expression of M1-like specific markers *Nlrp3*, *Cxcl2*, *Mmp9* was elevated in females, suggesting that these macrophages have an enhanced inflammatory phenotype in the atherosclerotic aorta of females compared to males (**Figure 5C**). Males, on the other hand, show increased presence of *Trem2*$^+$ myeloid cells including non-foamy M2-like macrophages (*Trem2*, *Mmp12*), foamy macrophages (*Fabp5*, *Cd5l*), resident M2 macrophages (*Lyve1*, *Mrc1*) and mixed *Trem2*$^+$ macrophages (*Emp1*, *Lpl*; **Figure 5A** and **Supplementary Table S5**). Foamy macrophages are characteristic of atherosclerotic plaques and are considered to be rather anti-inflammatory than pro-inflammatory.[12] *Cd36*, *Apoe*, *Fabp5*, and *Cd5l* expression was higher in male *Trem2*$^+$ foamy macrophages, which mediate lipid-uptake and promote foam cell survival in lesions (**Figure 5D** and **E**).[43,44] Additionally, male foamy macrophages showed increased expression of *Tgfb1* and *Gpnmb* (encoding a glycoprotein that is upregulated in foamy macrophages)[45], which have been described to regulate lesion development (**Figure 5E**). Cluster 7 consists of a mix of foamy and non-foamy macrophages with differential expression of *Lpl* and *Spp1* between males and females (**Supplementary Figure S6C**).

Conventional dendritic cells (cDCs; *Xcr1*, *Ppt1*) and migratory dendritic cells (mDCs; *Ccr7*, *Ccl5*, *Ccl17*, *Ccl22*) were more abundant in males (**Figure 5A**). Interestingly, male mDCs showed higher expression of chemokines *Ccl5* and *Ccl22* compared to females (**Supplementary Figure S6D**). Expression of MHCII-related genes (*H2-Aa*, *H2-Ab1*, *H2-Eb1*, *Ciita*) among the DC clusters was highest in the cDCs, but comparable between sexes (**Supplementary Figure S6E**). We identified cluster 5 and 10 as neutrophils (*Ly6g*, *Cd177*), of which cluster 10 seemed to be proliferating based on high expression of *Mki67* and histone-encoding genes (**Supplementary Table S5**). Although neutrophils in females showed elevated expression of pro-inflammatory gene *S100a8*, expression of other neutrophil markers were comparable (**Supplementary Figure S5D**). Mast cells (MCs) in cluster 9 showed comparable

gene expression levels of MC-markers *Fcer1a* and *Cpa3*, while c-Kit (*Kit*) was more expressed in females (**Figure 5F**). Although MC-specific protease genes encoding chymase (*Cma1*) and tryptase (*Tpsab1*) were barely detected, genes encoding secretory molecules *Ctsg*, *Ccl3*, *Ccl4* and antigen-presentation-associated molecules (*H2-Aa*/*Ab*/*Eb1*, *Cd74*) were increased in female MCs, suggesting a more pro-atherogenic signature of MCs in female compared to male aortas.

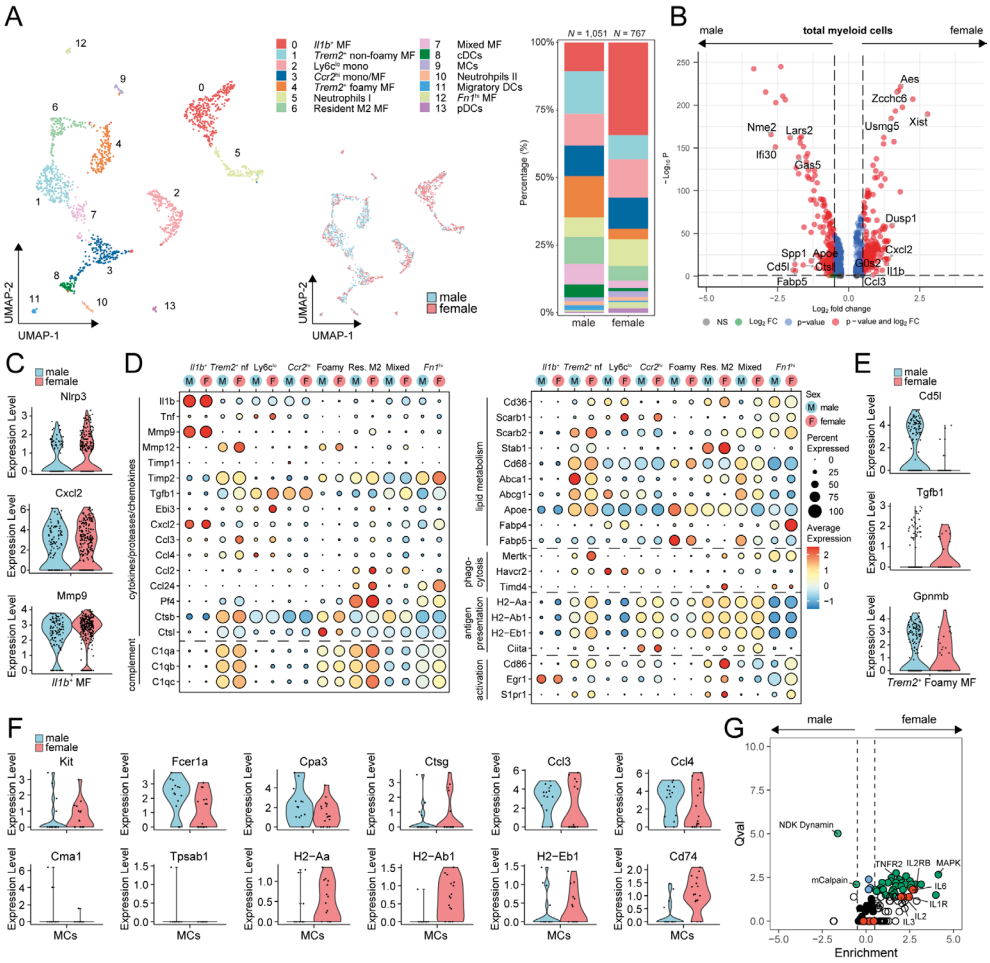


**Figure 5. Plaques of aged male and female *Ldlr*$^{-/-}$ mice differ in myeloid cell proportions. A)** UMAP plots and stacked diagram of myeloid cell clusters in the aorta of *Ldlr*$^{-/-}$ mice. **B)** Volcano plot displaying differentially expressed genes of the total myeloid cell cells between aged male and female *Ldlr*$^{-/-}$ mice. **C)** Sex-specific expression levels of *Il1b*$^{+}$ M1-associated genes. **D)** Dot plot displaying the sex-specific expression of biological process-associated genes in macrophage clusters. Sex-specific gene expression of **E)** *Trem2*$^{+}$ M2-related genes in cluster 4 and **F)** mast cell associated-markers in cluster 9. **G)** Pathway enrichment of myeloid cells in male and female mice. Green dots: significantly enriched pathways; red dots: interleukin-related pathways; white dots: insignificantly enriched pathways; black dots: insignificantly unenriched pathways.

Lastly, pathway analysis showed enrichment of the phagocytosis-associated NDK Dynamin pathway (*Nme2*, *Dnm1*), and the migration-associated Calpain pathway (*Cxcr3*, *Itgb1*, *Tln1*) in myeloid cells of males, while inflammatory signaling, such as interleukin-related (red dots: IL6, IL1R, IL2, IL2RB

pathways), MAPK and TNFR pathways, was enriched in female myeloid cells (**Figure 5G**).

## DISCUSSION

Advances in single-cell technologies have enabled comprehensive profiling of immune cell populations in the atherosclerotic plaque. While sex is known to impact immune responses and atherosclerotic CVD prevalence and manifestation, sex differences in the immune landscape of the plaque are rarely studied. Our study reveals sexual dimorphism in plaque composition and immune cell proportions and gene signatures in aged *Ldlr*$^{-/-}$ mice.

While plaques of young WD-fed male and female *Ldlr*$^{-/-}$ mice show no difference in collagen and necrotic core area[46,47], our data shows that plaques of aged female *Ldlr*$^{-/-}$ mice were relatively more stable compared to plaques of aged male *Ldlr*$^{-/-}$ mice, due to increased collagen content, and less necrotic core area and macrophages. This corroborates with studies in humans, in which female CVD patients display similar signs of plaque stability compared to male.[48] We did however observe a higher influx of immune cells in female compared to male atherosclerotic aortas of aged *Ldlr*$^{-/-}$ mice and found that gene expression of pro-atherogenic markers and inflammatory signaling pathways were more enriched in female aortas. In line with these findings, women are known to elicit stronger innate and adaptive immune responses compared to men, contributing to their increased susceptibility for inflammatory and autoimmune diseases.[49]



We report a striking increase of ABCs in aortas of atherosclerotic female mice, displaying enhanced expression of genes involved in B cell activation and antigen presentation, compared to ABCs in aortas of male atherosclerotic mice, which illustrates sex differences in B cell immunity that could contribute to atherosclerosis. We see enrichment of immunoglobulin genes in ABCs in addition to female-biased expression of *Tbx21* (T-bet) and *Cd72*, which are associated with autoantibody production.[50–52] Furthermore, expression of genes associated with plasma cell differentiation was elevated in female ABCs, suggesting that ABCs in females are more likely to become antibody-secreting cells in atherosclerosis. Accordingly, although only few plasma cells were found in the atherosclerotic aortas, their abundance was increased in females. High frequencies of ABCs in women have previously been linked to the susceptibility of autoimmune diseases, such as systemic lupus erythematosus , rheumatoid arthritis and multiple sclerosis.[34,35,53–56] Interestingly, both the *Tlr7* gene, crucial for ABC activation, and the gene for CD40L, which is involved in immunoglobulin class switching, are located on the X chromosome.[57] Since almost 15% of X-linked genes escape silencing, this may clarify the increased ABC frequency observed in females compared to males.[58] In addition, estrogen has been shown to stimulate the survival and activation of autoreactive B cells.[59–61] These findings contribute to the increasing body of evidence that atherosclerosis pathology involves autoimmune-like components[62–64], but where these age-associated B cells are precisely located in the atherosclerotic plaque environment remains to be investigated.

The presence of clonally expanded, activated T cells in the plaque of cardiovascular disease patients and mice also supports the concept of atherosclerosis as an inflammatory disease with autoimmune-like features.[65,66] Depuydt *et al.* showed that clonally expanded CD8$^{+}$ T cells in the plaque of male CVD

patients had increased expression of granzymes (*GZMB*, *GZMK* and *GZMA*) compared to $CD8^+$ T cells in the blood.[66] Although we did not investigate clonality of T cells in this study, we show that the immune landscape in males is more $CD8^+$ T cell-driven, illustrated by the large male-specific increase in $Gzmk^+CD8+$ T cells and $Gzmb^+CD8^+$ T cells. Both $CD8^+$ T cell populations express high levels of *Ccr5* and its ligand *Ccl5*, and in males show more expression of genes associated with activation and migration. Research has demonstrated that both antagonism and deficiency of the CCR5/CCL5-axis attenuate atherosclerosis in advanced stages by decreasing lesion size, promoting plaque stability, and reducing monocyte, macrophage, and T cell infiltration.[67,68] The male-specific increase in *Ccr5*-expressing $CD8^+$ T cells may contribute to the relatively increased macrophage content and reduced collagen that we observed in aged $Ldlr^{-/-}$ male mice. Furthermore, we observed elevated gene expression of activation marker *Cd69* across multiple T cell types in males[69], corroborating with high expression of *Cd69* on clonally expanded T cells and a large proportion of $CD69^+$ cells among T cells in plaques of male CVD patients.[66] $CD4^+CD8^+$ DP T cells accounted for the majority (~36%) of the T cells in females and have been previously found in murine and human plaques.[13,70] Possibly, these cells escaped from the thymus into the periphery promoted by age-induced thymic involution.[71] However, in contrast to immature $CD4^+CD8^+$ thymocytes[72], $CD4^+CD8^+$ DP T cells in the plaque show high expression of the cytolytic factor GzmA and memory markers. In line with these findings, $CD4^+CD8^+$ DP T cells with cytotoxic or regulatory functions have been described in viral infections[73,74], cancer[75,76] and rheumatoid arthritis.[77] Although some studies show that sex hormones can influence thymic involution and the number of $CD4^+$ $CD8^+$ DP T cells[78–82], Aspinall *et al.* have shown a sex hormone-independent increase in $CD4^+$ $CD8^+$ DP T cells in females.[83]

We found an increase in $CD11b^+$ myeloid cell numbers, including a larger proportion of conventional and migratory DCs, as well as $Trem2^+$ non-foamy M2-like macrophages in aortas of aged males, while the female myeloid compartment largely contained pro-inflammatory $Il1b^+$ M1-like macrophages. Elevated expression of foam cell survival genes in the male $Trem2^+$ foamy macrophage cluster may explain the increase in foamy macrophage proportion and larger macrophage area observed in male lesions. In addition, increased expression of *Tgfb1* and *Gpnmb* in this cluster may contribute to regulating plaque development in the male mice.[44] We observed a higher M1/M2 macrophage ratio in atherosclerotic plaques of females than in males. In autoimmune diseases such as SLE and RA, females also show a bias towards M1 polarization, however the underlying mechanism is unclear.[84] Notably, mast cells displayed a more pro-atherogenic gene profile in female compared to male mice as illustrated by increased expression of proteases, chemokines and MHC class II molecules. This is in line with a previous study which showed that mast cells in females store and secrete more inflammatory mediators and are more likely to initiate an immune response.[85]

Although limited conclusive information is available on how hormonal and chromosomal sex differences affect inflammation in atherosclerosis, a variety of studies highlighted the impact of estrogen on leukocyte migration. Estrogen inhibited IL-1-induced upregulation of ICAM-1 and VCAM-1 human endothelial cells[86], and reduced MCP-1 expression in rabbits.[87] These estrogen-related effects might decrease monocyte chemotaxis in atherosclerosis, thereby possibly leading to the lower macrophage content in females compared to males. Furthermore, men with androgen deficiencies have higher IL-

1β concentrations than men with normal testosterone levels[88,89], which might contribute to the lower proportion of inflammatory *Il1b*$^{+}$ macrophages in males compared to females.

It should however be noted that female mice do not experience a dramatic reduction in estrogen levels that resembles human menopause, but have comparable estrogen levels during aging.[90] These endocrinologic differences between mice and men, in addition to dissimilarities in the aging environment between laboratory mice and humans, are limitations of using preclinical models.[91–94]Apart from biological differences, it is important to keep in mind that our study faced several technical limitations. The limited number of aortic immune cells demands pooling of multiple samples to obtain enough events for single-cell RNA sequencing analysis, which restrained us from performing statistical analysis and may affect differential gene expression profiles. In addition, although we thoroughly cleaned and flushed the aorta, we cannot exclude contamination with a few circulating leukocytes. Nevertheless, our single-cell RNA sequencing analysis and validation at protein level using flow cytometry reveal an elaborate insight into immunological differences between aged atherosclerotic male and female mice, which should be taken into account in preclinical atherosclerosis research.



## CONCLUSION

Our data can be utilized as a valuable tool for future preclinical studies, including target validation in experimental mice for intervention studies, but also in refining study design and rationale for choosing the appropriate sex. Although we cannot not directly extrapolate the observed sex differences in the murine atherosclerotic immune landscape to that of humans, we do see similarities between the aged *Ldlr*$^{-/-}$ mouse model and human atherosclerosis pathology, illustrating the relevance of our data set.

Taken together, our study shows that sex is a variable that influences plaque characteristics and immune cell composition at single-cell resolution in aged *Ldlr*$^{-/-}$ mice. These immunological sex differences may contribute to sex-based clinical differences in atherosclerotic CVD and highlight potential future areas of sex-specific immunomodulating therapies to combat atherosclerosis. To investigate this, further research into sex differences of the immune landscape of atherosclerotic plaques of cardiovascular disease patients is needed.

## DATA AVAILABILITY

*In silico* data analysis was performed using custom R scripts (R version 4.1.2) designed especially for this research and/or based on the recommended pipelines from the pre-existing packages listed in the individual segments above. Single-cell RNA sequencing data are available upon personal request from the corresponding author (a.c.foks@lacdr.leidenuniv.nl).

## COMPETING INTERESTS

The authors declare that they have no competing interests.

## FUNDING

This work was supported by the Dutch Heart Foundation grant number 2018T051 to A.C.F., 2019T067 to I.B., CVON2017-20: Generating the best evidence-based pharmaceutical targets and drugs for atherosclerosis (GENIUS II) to J.K, and the ERA-CVD B-eatATHERO consortium; Dutch Heart Foundation grant number 2019T107 to A.C.F.

## AUTHORS' CONTRIBUTIONS

V.S. and A.C.F. participated in the conceptualization and performed data analysis. V.S., J.d.M. and A.C.F. drafted the manuscript and designed the figures. V.S., J.d.M., M.N.A.B.K., M.A.C.D., I.B., and A.C.F executed the animal experiments. All authors provided feedback on the research, analyses and manuscript.

## ACKNOWLEDGEMENTS

We would like to thank Berend from the Flow Cytometry Core Facility and Marja from the Genomics Core Facility of the AMC for flow sorting and processing the samples for sequencing. Graphical abstract and experimental set-up in Figure 1 and 2 were created with BioRender.com.

# REFERENCES


1. Timmis A, Vardas P, Townsend N, Torbica A, Katus H, De Smedt D, Gale CP, Maggioni AP, Petersen SE, Huculeci R, Kazakiewicz D, de Benito Rubio V, Ignatiuk B, Raisi-Estabragh Z, Pawlak A, Karagiannidis E, Treskes R, Gaita D, Beltrame JF, McConnachie A, Bardinet I, Graham I, Flather M, Elliott P, Mossialos EA, Weidinger F, Achenbach S. European Society of Cardiology: cardiovascular disease statistics 2021. Eur Heart J. 2022;43:716–799.
2. Towfighi A, Zheng L, Ovbiagele B. Sex-specific trends in midlife coronary heart disease risk and prevalence. Arch Intern Med. 2009;169:1762–1766.
3. Tsao CW, Aday AW, Almarzooq ZI, Anderson CAM, Arora P, Avery CL, Baker-Smith CM, Beaton AZ, Boehme AK, Buxton AE, Commodore-Mensah Y, Elkind MSV, Evenson KR, Eze-Nliam C, Fugar S, Generoso G, Heard DG, Hiremath S, Ho JE, Kalani R, Kazi DS, Ko D, Levine DA, Liu J, Ma J, Magnani JW, Michos ED, Mussolino ME, Navaneethan SD, Parikh NI, Poudel R, Rezk-Hanna M, Roth GA, Shah NS, St-Onge MP, Thacker EL, Virani SS, Voeks JH, Wang NY, Wong ND, Wong SS, Yaffe K, Martin SS. Heart Disease and Stroke Statistics-2023 Update: A Report From the American Heart Association. Circulation. 2023;147:E93–E621.
4. Di Giosia P, Passacquale G, Petrarca M, Giorgini P, Marra AM, Ferro A. Gender differences in cardiovascular prophylaxis: Focus on antiplatelet treatment. Pharmacol Res. 2017;119:36–47.
5. Vrijenhoek JEP, Den Ruijter HM, De Borst GJ, De Kleijn DPV, De Vries JPPM, Bots ML, Van De Weg SM, Vink A, Moll FL, Pasterkamp G. Sex is associated with the presence of atherosclerotic plaque hemorrhage and modifies the relation between plaque hemorrhage and cardiovascular outcome. Stroke. 2013;44:3318–3323.
6. Lansky AJ, Ng VG, Maehara A, Weisz G, Lerman A, Mintz GS, De Bruyne B, Farhat N, Niess G, Jankovic I, Lazar D, Xu K, Fahy M, Serruys PW, Stone GW. Gender and the extent of coronary atherosclerosis, plaque composition, and clinical outcomes in acute coronary syndromes. JACC Cardiovasc Imaging. 2012;5.
7. Halvorsen DS, Johnsen SH, Mathiesen EB, Njølstad I. The association between inflammatory markers and carotid atherosclerosis is sex dependent: the Tromsø Study. Cerebrovasc Dis. 2009;27:392–397.
8. Sato T, Minami Y, Asakura K, Katamine M, Kato A, Katsura A, Muramatsu Y, Kakizaki R, Nemoto T, Hashimoto T, Fujiyoshi K, Kameda R, Meguro K, Shimohama T, Ako J. Age- and Gender-Related Differences in Coronary Lesion Plaque Composition on Optical Coherence Tomography. Circ J. 2020;84:463–470.
9. Maas AHEM, Appelman YEA. Gender differences in coronary heart disease. Neth Heart J. 2010;18:598–603.
10. Winkels H, Ehinger E, Vassallo M, Buscher K, Dinh HQ, Kobiyama K, Hamers AAJ, Cochain C, Vafadarnejad E, Saliba AE, Zernecke A, Pramod AB, Ghosh AK, Michel NA, Hoppe N, Hilgendorf I, Zirlik A, Hedrick CC, Ley K, Wolf D. Atlas of the immune cell repertoire in mouse atherosclerosis defined by single-cell RNA-sequencing and mass cytometry. Circ Res. 2018;122:1675–1688.
11. Cochain C, Vafadarnejad E, Arampatzi P, Pelisek J, Winkels H, Ley K, Wolf D, Saliba AE, Zernecke A. Single-Cell RNA-Seq Reveals the Transcriptional Landscape and Heterogeneity of Aortic Macrophages in Murine Atherosclerosis. Circ Res. 2018;122:1661–1674.
12. Kim K, Shim D, Lee JS, Zaitsev K, Williams JW, Kim KW, Jang MY, Jang HS, Yun TJ, Lee SH, Yoon WK, Prat A, Seidah NG, Choi J, Lee SP, Yoon SH, Nam JW, Seong JK, Oh GT, Randolph GJ, Artyomov MN, Cheong C, Choi JH. Transcriptome Analysis Reveals Nonfoamy Rather Than Foamy Plaque Macrophages Are Proinflammatory in Atherosclerotic Murine Models. Circ Res. 2018;123:1127–1142.
13. Fernandez DM, Rahman AH, Fernandez NF, Chudnovskiy A, Amir E ad D, Amadori L, Khan NS, Wong CK, Shamailova R, Hill CA, Wang Z, Remark R, Li JR, Pina C, Faries C, Awad AJ, Moss N, Bjorkegren JLM, Kim-Schulze S, Gnjatic S, Ma'ayan A, Mocco J, Faries P, Merad M, Giannarelli C. Single-cell immune landscape of human atherosclerotic plaques. Nat Med. 2019;25:1576–1588.
14. Depuydt MAC, Prange KHM, Slenders L, Örd T, Elbersen D, Boltjes A, De Jager SCA, Asselbergs FW, De Borst GJ, Aavik E, Lönnberg T, Lutgens E, Glass CK, Den Ruijter HM, Kaikkonen MU, Bot I, Slütter B, Van Der Laan SW, Yla-Herttuala S, Mokry M, Kuiper J, De Winther MPJ, Pasterkamp G. Microanatomy of the Human Atherosclerotic Plaque by Single-Cell Transcriptomics. Circ Res. 2020;127:1437–1455.
15. Smit V, de Mol J, Schaftenaar FH, Depuydt MAC, Postel RJ, Smeets D, Verheijen FWM, Bogers L, van Duijn J, Verwilligen RAF, Grievink HW, Bernabé Kleijn MNA, van Ingen E, de Jong MJM, Goncalves L, Peeters JAHM, Smeets HJ, Wezel A, Polansky JK, de Winther MPJ, Binder CJ, Tsiantoulas D, Bot I, Kuiper J, Foks AC. Single-cell profiling reveals age-associated immunity in atherosclerosis. Cardiovasc Res. 2023;
16. Hartman RJG, Owsiany K, Ma L, Koplev S, Hao K, Slenders L, Civelek M, Mokry M, Kovacic JC, Pasterkamp G, Owens G, Björkegren JLM, Den Ruijter HM. Sex-Stratified Gene Regulatory Networks Reveal Female Key Driver Genes of Atherosclerosis Involved in Smooth Muscle Cell Phenotype Switching. Circulation. 2021;143:713–726.
17. Elizabeth Moss M, Lu Q, Iyer SL, Engelbertsen D, Marzolla V, Caprio M, Lichtman AH, Jaffe IZ. Endothelial Mineralocorticoid Receptors Contribute to Vascular Inflammation in Atherosclerosis in a Sex-Specific Manner. Arterioscler Thromb Vasc Biol. 2019;39:1588–1601.
18. Engel D, Beckers L, Wijnands E, Seijkens T, Lievens D, Drechsler M, Gerdes N, Soehnlein O, Mat †, Daemen JAP, Stan R V, Biessen EAL, Lutgens E. Caveolin-1 deficiency decreases atherosclerosis by hampering leukocyte influx into the arterial wall and generating a regulatory T-cell response. FASEB J. 2011;25:3838–3848.
19. Hernández-Vargas P, Ortiz-Muñoz G, López-Franco O, Suzuki Y, Gallego-Delgado J, Sanjuán G, Lázaro A, López-Parra V, Ortega L, Egido J, Gómez-Guerrero C. Fcγ Receptor Deficiency Confers Protection Against Atherosclerosis in Apolipoprotein E Knockout Mice. Circ Res. 2006;99:1188–1196.

20. Smith DD, Tan X, Tawfik O, Milne G, Stechschulte DJ, Dileepan KN. Increased Aortic Atherosclerotic Plaque Development In Female Apolipoprotein E-null Mice Is Associated With Elevated Thromboxane A2 And Decreased Prostacyclin Production. J Physiol Pharmacol. 2010;61:309.
21. Rodgers JL, Jones J, Bolleddu SI, Vanthenapalli S, Rodgers LE, Shah K, Karia K, Panguluri SK. Cardiovascular Risks Associated with Gender and Aging. J Cardiovasc Dev Dis. 2019;6:19.
22. Vos A, de Jong PA, Verdoorn D, Mali WPTM, Bleys RLAW, Vink A. Histopathological characterization of intimal lesions and arterial wall calcification in the arteries of the leg of elderly cadavers. Clin Anat. 2021;34:835.
23. Saul D, Kosinsky RL, Atkinson EJ, Doolittle ML, Zhang X, LeBrasseur NK, Pignolo RJ, Robbins PD, Niedernhofer LJ, Ikeno Y, Jurk D, Passos JF, Hickson LTJ, Xue A, Monroe DG, Tchkonia T, Kirkland JL, Farr JN, Khosla S. A new gene set identifies senescent cells and predicts senescence-associated pathways across tissues. Nat Commun. 2022;13.
24. Aibar S, González-Blas CB, Moerman T, Huynh-Thu VA, Imrichova H, Hulselmans G, Rambow F, Marine JC, Geurts P, Aerts J, Van Den Oord J, Atak ZK, Wouters J, Aerts S. SCENIC: single-cell regulatory network inference and clustering. Nat Methods. 2017;14:1083–1086.
25. Bibby JA, Agarwal D, Freiwald T, Kunz N, Merle NS, West EE, Singh P, Larochelle A, Chinian F, Mukherjee S, Afzali B, Kemper C, Zhang NR. Systematic single-cell pathway analysis to characterize early T cell activation. Cell Rep. 2022;41.
26. Elgueta R, Benson MJ, De Vries VC, Wasiuk A, Guo Y, Noelle RJ. Molecular mechanism and function of CD40/CD40L engagement in the immune system. Immunol. Rev. 2009;229:152–172.
27. Krzyzak L, Seitz C, Urbat A, Hutzler S, Ostalecki C, Gläsner J, Hiergeist A, Gessner A, Winkler TH, Steinkasserer A, Nitschke L. CD83 Modulates B Cell Activation and Germinal Center Responses. J Immunol. 2016;196:3581–3594.
28. Axelsson S, Magnuson A, Lange A, Alshamari A, Hörnquist EH, Hultgren O. A combination of the activation marker CD86 and the immune checkpoint marker B and T lymphocyte attenuator (BTLA) indicates a putative permissive activation state of B cell subtypes in healthy blood donors independent of age and sex. BMC Immunol. 2020;21.
29. Gururajan M, Simmons A, Dasu T, Spear BT, Calulot C, Robertson DA, Wiest DL, Monroe JG, Bondada S. Early growth response genes regulate B cell development, proliferation, and immune response. J Immunol. 2008;181:4590–4602.
30. Chaplin JW, Kasahara S, Clark EA, Ledbetter JA. Anti-CD180 (RP105) activates B cells to rapidly produce polyclonal Ig via a T cell and MyD88-independent pathway. J Immunol. 2011;187:4199.
31. Sunshine A, Goich D, Stith A, Sortino K, Dalton J, Metcalfe S, Svensson EC, Garrett-Sinha LA. Ets1 Controls the Development of B Cell Autoimmune Responses in a Cell-Intrinsic Manner. Immunohorizons. 2019;3:331–340.
32. Schittenhelm L, Hilkens CM, Morrison VL. β2 Integrins As Regulators of Dendritic Cell, Monocyte, and Macrophage Function. Front Immunol. 2017;8.
33. Wu HJ, Bondada S. CD72, a coreceptor with both positive and negative effects on B lymphocyte development and function. J Clin Immunol. 2009;29:12–21.
34. Mouat IC, Goldberg E, Horwitz MS. Age-associated B cells in autoimmune diseases. Cell Mol Life Sci. 2022;79.
35. van Langelaar J, Rijvers L, Janssen M, Wierenga-Wolf AF, Melief MJ, Siepman TA, de Vries HE, Unger PPA, van Ham SM, Hintzen RQ, van Luijn MM. Induction of brain-infiltrating T-bet–expressing B cells in multiple sclerosis. Ann Neurol. 2019;86:264–278.
36. Yoon HS, Scharer CD, Majumder P, Davis CW, Butler R, Zinzow-Kramer W, Skountzou I, Koutsonanos DG, Ahmed R, Boss JM. ZBTB32 is an early repressor of the CIITA and MHC class II gene expression during B cell differentiation to plasma cells. J Immunol. 2012;189:2393–2403.
37. Chevrier S, Emslie D, Shi W, Kratina T, Wellard C, Karnowski A, Erikci E, Smyth GK, Chowdhury K, Tarlinton D, Corcoran LM. The BTB-ZF transcription factor Zbtb20 is driven by Irf4 to promote plasma cell differentiation and longevity. J Exp Med. 2014;211:827–840.
38. Wrammert J, Källberg E, Agace WW, Leanderson T. Ly6C expression differentiates plasma cells from other B cell subsets in mice.
39. Yang Y, Li X, Ma Z, Wang C, Yang Q, Byrne-Steele M, Hong R, Min Q, Zhou G, Cheng Y, Qin G, Youngyunpipatkul J V., Wing JB, Sakaguchi S, Toonstra C, Wang LX, Vilches-Moure JG, Wang D, Snyder MP, Wang JY, Han J, Herzenberg LA. CTLA-4 expression by B-1a B cells is essential for immune tolerance. Nat Commun. 2021;12.
40. Wilson TJ, Clare S, Mikulin J, Johnson CM, Harcourt K, Lyons PA, Dougan G, Smith KGC. Signalling lymphocyte activation molecule family member 9 is found on select subsets of antigen-presenting cells and promotes resistance to Salmonella infection. Immunology. 2020;159:393.
41. Gorfu G, Rivera-Nieves J, Hoang S, Abbott DW, Arbenz-Smith K, Azar DW, Pizarro TT, Cominelli F, McDuffie M, Ley K. Beta7 integrin deficiency suppresses B cell homing and attenuates chronic ileitis in SAMP1/YitFc mice. J Immunol. 2010;185:5561–5568.
42. Sato Y, Oguchi A, Fukushima Y, Masuda K, Toriu N, Taniguchi K, Yoshikawa T, Cui X, Kondo M, Hosoi T, Komidori S, Shimizu Y, Fujita H, Jiang L, Kong Y, Yamanashi T, Seita J, Yamamoto T, Toyokuni S, Hamazaki Y, Hattori M, Yoshikai Y, Boor P, Floege J, Kawamoto H, Murakawa Y, Minato N, Yanagita M. CD153/CD30 signaling promotes age-dependent tertiary lymphoid tissue expansion and kidney injury. J Clin Invest. 2022;132.
43. Arai S, Shelton JM, Chen M, Bradley MN, Castrillo A, Bookout AL, Mak PA, Edwards PA, Mangelsdorf DJ, Tontonoz P, Miyazaki T. A role for the apoptosis inhibitory factor AIM/Spalpha/Api6 in atherosclerosis development. Cell Metab. 2005;1:201–213.
44. Amézaga N, Sanjurjo L, Julve J, Aran G, Pérez-Cabezas B, Bastos-Amador P, Armengol C, Vilella R, Escolà-Gil JC, Blanco-Vaca F, Borràs FE, Valledor AF, Sarrias M-R. Human scavenger protein AIM increases foam cell formation and CD36-mediated oxLDL uptake. J Leukoc Biol. 2014;95:509–520.

45. Nickl B, Qadri F, Bader M. Role of Gpnmb in atherosclerosis of female mice. Biochem Biophys Res Commun. 2022;621:20–24.
46. Petrovan RJ, Kaplan CD, Reisfeld RA, Curtiss LK. DNA vaccination against VEGF receptor 2 reduces atherosclerosis in LDL receptor-deficient mice. Arterioscler Thromb Vasc Biol. 2007;27:1095–1100.
47. Sala F, Aranda JF, Rotllan N, Ramírez CM, Aryal B, Elia L, Condorelli G, Catapano AL, Fernández-Hernando C, Norata GD. MiR-143/145 deficiency attenuates the progression of atherosclerosis in Ldlr-/-mice. Thromb Haemost. 2014;112:796–802.
48. Man JJ, Beckman JA, Jaffe IZ. Sex as a Biological Variable in Atherosclerosis. Circ Res. 2020;126:1297–1319.
49. Klein SL, Flanagan KL. Sex differences in immune responses. Nat Rev Immunol. 2016;16:626–638.
50. Shen Y, Ma Y, Xie J, Lin L, Shi Y, Li X, Shen P, Pan X, Ren H. A regulatory role for CD72 expression on B cells and increased soluble CD72 in primary Sjogren's syndrome. BMC Immunol. 2020;21:1–6.
51. Peng SL, Szabo SJ, Glimcher LH. T-bet regulates IgG class switching and pathogenic autoantibody production. Proc Natl Acad Sci U S A. 2002;99:5545–5550.
52. Rubtsova K, Rubtsov A V., Thurman JM, Mennona JM, Kappler JW, Marrack P. B cells expressing the transcription factor T-bet drive lupus-like autoimmunity. J Clin Invest. 2017;127:1392–1404.
53. Ricker E, Manni M, Flores-Castro D, Jenkins D, Gupta S, Rivera-Correa J, Meng W, Rosenfeld AM, Pannellini T, Bachu M, Chinenov Y, Sculco PK, Jessberger R, Prak ETL, Pernis AB. Altered function and differentiation of age-associated B cells contribute to the female bias in lupus mice. Nat Commun. 2021;12.
54. Rubtsov A V., Rubtsova K, Fischer A, Meehan RT, Gillis JZ, Kappler JW, Marrack P. Toll-like receptor 7 (TLR7)-driven accumulation of a novel CD11c+ B-cell population is important for the development of autoimmunity. Blood. 2011;118:1305–1315.
55. Wang S, Wang J, Kumar V, Karnell JL, Naiman B, Gross PS, Rahman S, Zerrouki K, Hanna R, Morehouse C, Holoweckyj N, Liu H, Casey K, Smith M, Parker M, White N, Riggs J, Ward B, Bhat G, Rajan B, Grady R, Groves C, Manna Z, Goldbach-Mansky R, Hasni S, Siegel R, Sanjuan M, Streicher K, Cancro MP, Kolbeck R, Ettinger R. IL-21 drives expansion and plasma cell differentiation of autoreactive CD11chiT-bet+ B cells in SLE. Nat Commun. 2018;9:1–14.
56. Qin Y, Cai ML, Jin HZ, Huang W, Zhu C, Bozec A, Huang J, Chen Z. Age-associated B cells contribute to the pathogenesis of rheumatoid arthritis by inducing activation of fibroblast-like synoviocytes via TNF-α-mediated ERK1/2 and JAK-STAT1 pathways. Ann Rheum Dis. 2022;81:1504–1514.
57. Sarmiento L, Svensson J, Barchetta I, Giwercman A, Cilio CM. Copy number of the X-linked genes TLR7 and CD40L influences innate and adaptive immune responses. Scand J Immunol. 2019;90.
58. Pinheiro I, Dejager L, Libert C. X-chromosome-located microRNAs in immunity: might they explain male/female differences? The X chromosome-genomic context may affect X-located miRNAs and downstream signaling, thereby contributing to the enhanced immune response of females. Bioessays. 2011;33:791–802.
59. Jeganathan V, Peeva E, Diamond B. Hormonal milieu at time of B cell activation controls duration of autoantibody response. J Autoimmun. 2014;53:46–54.
60. Grimaldi CM, Jeganathan V, Diamond B. Hormonal regulation of B cell development: 17 beta-estradiol impairs negative selection of high-affinity DNA-reactive B cells at more than one developmental checkpoint. J Immunol. 2006;176:2703–2710.
61. Grimaldi CM, Michael DJ, Diamond B. Cutting edge: expansion and activation of a population of autoreactive marginal zone B cells in a model of estrogen-induced lupus. J Immunol. 2001;167:1886–1890.
62. Lorenzo C, Delgado P, Busse CE, Sanz-Bravo A, Martos-Folgado I, Bonzon-Kulichenko E, Ferrarini A, Gonzalez-Valdes IB, Mur SM, Roldán-Montero R, Martinez-Lopez D, Martin-Ventura JL, Vázquez J, Wardemann H, Ramiro AR. ALDH4A1 is an atherosclerosis auto-antigen targeted by protective antibodies. Nature. 2021;589.
63. Palinski W, Hörkkö S, Miller E, Steinbrecher UP, Powell HC, Curtiss LK, Witztum JL. Cloning of Monoclonal Autoantibodies to Epitopes of Oxidized Lipoproteins from Apolipoprotein E-deficient Mice Demonstration of Epitopes of Oxidized Low Density Lipoprotein in Human Plasma modified lipo-proteins • autoantibodies • atherosclerosis • immune system. 1996.
64. Greco TP, Conti-Kelly AM, Anthony JR, Greco T, Doyle R, Boisen M, Kojima K, Matsuura E, Lopez LR. Oxidized-LDL/beta(2)-glycoprotein I complexes are associated with disease severity and increased risk for adverse outcomes in patients with acute coronary syndromes. Am J Clin Pathol. 2010;133:737–743.
65. Wang Z, Zhang X, Lu S, Zhang C, Ma Z, Su R, Li Y, Sun T, Li Y, Hong M, Deng X, Rafiee Monjezi M, Hristov M, Steffens S, Santovito D, Dornmair K, Ley K, Weber C, Mohanta SK, Habenicht AJR, Yin C. Pairing of single-cell RNA analysis and T cell antigen receptor profiling indicates breakdown of T cell tolerance checkpoints in atherosclerosis. Nat Cardiovasc Res 2023 23. 2023;2:290–306.
66. Depuydt MAC, Schaftenaar FH, Prange KHM, Boltjes A, Hemme E, Delfos L, de Mol J, de Jong MJM, Bernabé Kleijn MNA, Peeters JAHM, Goncalves L, Wezel A, Smeets HJ, de Borst GJ, Foks AC, Pasterkamp G, de Winther MPJ, Kuiper J, Bot I, Slütter B. Single-cell T cell receptor sequencing of paired human atherosclerotic plaques and blood reveals autoimmune-like features of expanded effector T cells. Nat Cardiovasc Res 2023 22. 2023;2:112–125.
67. Braunersreuther V, Zernecke A, Arnaud C, Liehn EA, Steffens S, Shagdarsuren E, Bidzhekov K, Burger F, Pelli G, Luckow B, Mach F, Weber C. Ccr5 but not Ccr1 deficiency reduces development of diet-induced atherosclerosis in mice. Arterioscler Thromb Vasc Biol. 2007;27:373–379.
68. Veillard NR, Kwak B, Pelli G, Mulhaupt F, James RW, Proudfoot AEI, Mach F. Antagonism of RANTES Receptors Reduces Atherosclerotic Plaque Formation in Mice. 2004;
69. Cibrián D, Sánchez-Madrid F. CD69: from activation marker to metabolic gatekeeper. Eur J Immunol. 2017;47:946–953.

70. Zernecke A, Winkels H, Cochain C, Williams JW, Wolf D, Soehnlein O, Robbins CS, Monaco C, Park I, McNamara CA, Binder CJ, Cybulsky MI, Scipione CA, Hedrick CC, Galkina E V., Kyaw T, Ghosheh Y, Dinh HQ, Ley K. Meta-Analysis of Leukocyte Diversity in Atherosclerotic Mouse Aortas. Circ Res. 2020;127:402–426.
71. Lee W-W, Nam K-H, Terao K, Akari H, Yoshikawa Y. Age-related increase of peripheral CD4+ CD8+ double-positive T lymphocytes in cynomolgus monkeys: longitudinal study in relation to thymic involution. Immunology. 2003;109:217–225.
72. Ebnet K, Levelt CN, Tran TT, Eichmann K, Simon MM. Transcription of granzyme A and B genes is differentially regulated during lymphoid ontogeny. J Exp Med. 1995;181:755–763.
73. Kitchen SG, Whitmire JK, Jones NR, Galic Z, Kitchen CMR, Ahmed R, Zack JA. The CD4 molecule on CD8+ T lymphocytes directly enhances the immune response to viral and cellular antigens. Proc Natl Acad Sci U S A. 2005;102:3794–3799.
74. Kitchen SG, Jones NR, LaForge S, Whitmire JK, Vu BA, Galic Z, Brooks DG, Brown SJ, Kitchen CMR, Zack JA. CD4 on CD8+ T cells directly enhances effector function and is a target for HIV infection. Proc Natl Acad Sci U S A. 2004;101:8727–8732.
75. Desfrançois J, Moreau-Aubry A, Vignard V, Godet Y, Khammari A, Dréno B, Jotereau F, Gervois N. Double Positive CD4CD8 αβ T Cells: A New Tumor-Reactive Population in Human Melanomas. PLoS One. 2010;5:e8437.
76. Rahemtullah A, Reichard KK, Preffer FI, Harris NL, Hasserjian RP. A Double-Positive CD4+CD8+ T-Cell Population Is Commonly Found in Nodular Lymphocyte Predominant Hodgkin Lymphoma. Am J Clin Pathol. 2006;126:805.
77. Quandt D, Rothe K, Scholz R, Baerwald CW, Wagner U. Peripheral CD4CD8 Double Positive T Cells with a Distinct Helper Cytokine Profile Are Increased in Rheumatoid Arthritis. PLoS One. 2014;9:e93293.
78. Zoller AL, Kersh GJ. Estrogen induces thymic atrophy by eliminating early thymic progenitors and inhibiting proliferation of beta-selected thymocytes. J Immunol. 2006;176:7371–7378.
79. Okasha SA, Ryu S, Do Y, McKallip RJ, Nagarkatti M, Nagarkatti PS. Evidence for estradiol-induced apoptosis and dysregulated T cell maturation in the thymus. Toxicology. 2001;163:49–62.
80. Bernardi AI, Andersson A, Stubelius A, Grahnemo L, Carlsten H, Islander U. Selective estrogen receptor modulators in T cell development and T cell dependent inflammation. Immunobiology. 2015;220:1122–1128.
81. Erlandsson MC, Ohlsson C, Gustafsson JÅ, Carlsten H. Role of oestrogen receptors alpha and beta in immune organ development and in oestrogen-mediated effects on thymus. Immunology. 2001;103:17–25.
82. Guevara Patiño JA, Marino MW, Ivanov VN, Nikolich-ˇ Zugich J. Sex steroids induce apoptosis of CD8 + CD4 + double-positive thymocytes via TNF-alpha. Eur Heart J. 30:2586–92.
83. Aspinall R, Andrew D, London R, 9nh S. Gender-Related Differences in the Rates of Age Associated Thymic Atrophy. Dev Immunol. 2001;8:95–106.
84. Funes SC, Rios M, Escobar-Vera J, Kalergis AM. Implications of macrophage polarization in autoimmunity. Immunology. 2018;154:186–195.
85. Mackey E, Ayyadurai S, Pohl CS, D'Costa S, Li Y, Moeser AJ. Sexual dimorphism in the mast cell transcriptome and the pathophysiological responses to immunological and psychological stress. Biol Sex Differ. 2016;7:1–19.
86. Caulin-Glaser T, Watson CA, Pardi R, Bender JR. Effects of 17beta-estradiol on cytokine-induced endothelial cell adhesion molecule expression. J Clin Invest. 1996;98:36–42.
87. Pervin S, Singh R, Rosenfeld ME, Navab M, Chaudhuri G, Nathan L. Estradiol suppresses MCP-1 expression In vivo : implications for atherosclerosis. Arterioscler Thromb Vasc Biol. 1998;18:1575–1582.
88. Mohamad NV, Wong SK, Wan Hasan WN, Jolly JJ, Nur-Farhana MF, Ima-Nirwana S, Chin KY. The relationship between circulating testosterone and inflammatory cytokines in men. Aging Male. 2019;22:129–140.
89. Chin KY, Ima-Nirwana S. The Effects of Testosterone Deficiency and Its Replacement on Inflammatory Markers in Rats: A Pilot Study. Int J Endocrinol Metab 2017 151. 2017;15:43053.
90. Dubal DB, Broestl L, Worden K. Sex and gonadal hormones in mouse models of Alzheimer's disease: what is relevant to the human condition? Biol Sex Differ. 2012;3:24.
91. Huggins MA, Jameson SC, Hamilton SE. Embracing microbial exposure in mouse research. J Leukoc Biol. 2019;105:73.
92. Li Y, Baldridge MT. Modelling human immune responses using microbial exposures in rodents. Nat Microbiol 2023 83. 2023;8:363–366.
93. Tao L, Reese TA. Making Mouse Models That Reflect Human Immune Responses. Trends Immunol. 2017;38:181–193.
94. Sanders AE, Arnesen H, Shepherd FK, Putri DS, Fiege JK, Pierson MJ, Roach SN, Carlsen H, Masopust D, Boysen P, Langlois RA. Comparison of mouse models of microbial experience reveals differences in microbial diversity and response to vaccination. mSphere. 2024;9.

# SUPPLEMENTARY MATERIAL

## SUPPLEMENTARY FIGURES

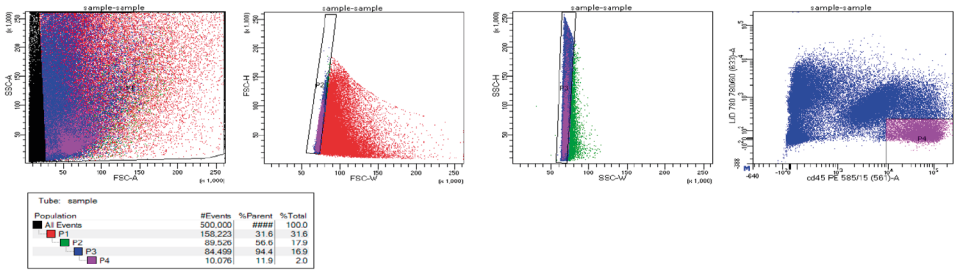


**Supplementary Figure S1. Gating scheme of aortic CD45$^+$ cells from male aged *Ldlr*$^{-/-}$ mice before single-cell RNA sequencing.** Gating strategy of alive aortic CD45$^+$ cells for sorting from chow diet-fed aged male *Ldlr*$^{-/-}$ mice.

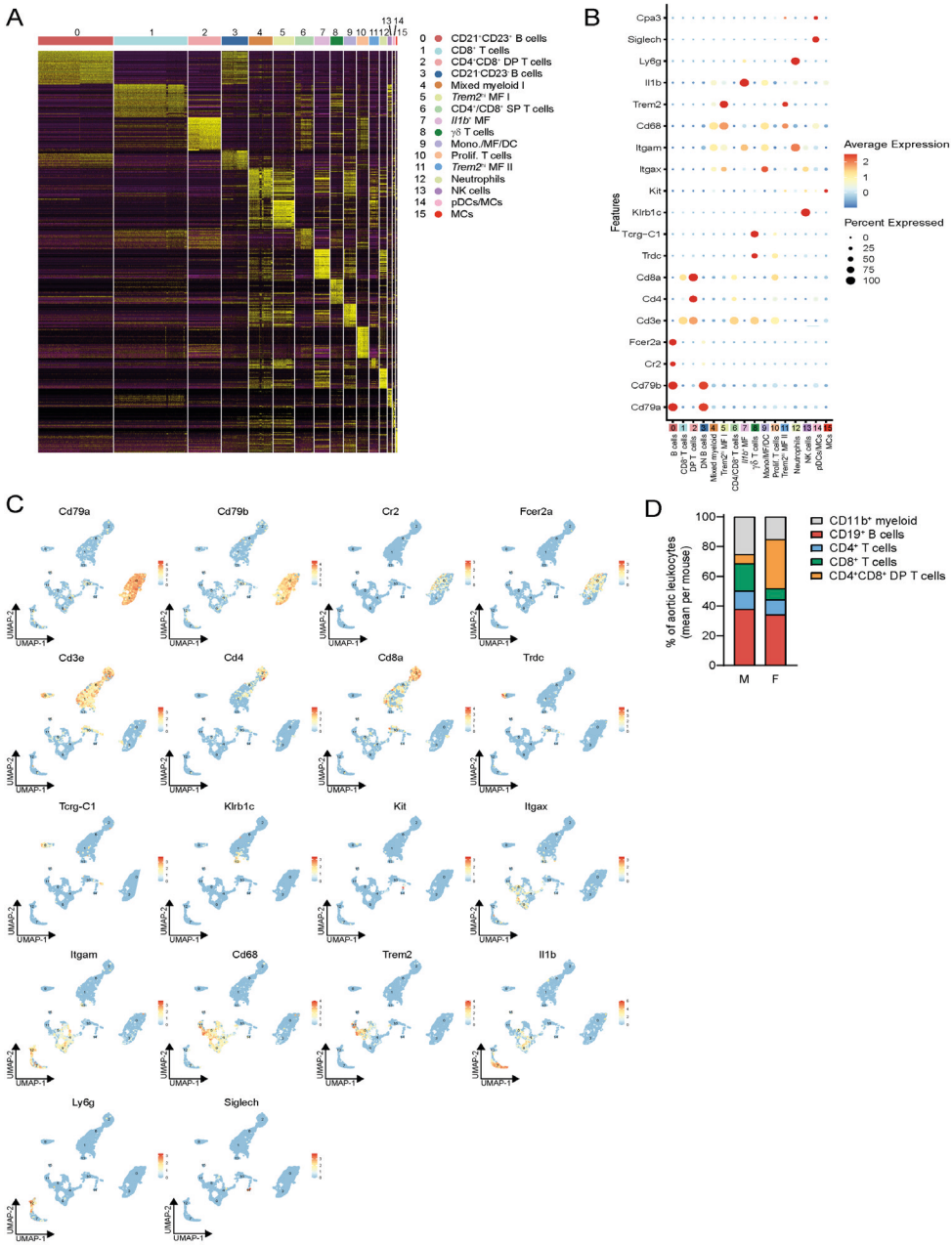


**Supplementary Figure S2. Immune cell clustering and frequency in aortas of aged *Ldlr*$^{-/-}$ mice. A)** Heatmap of the top 50 differentially expressed genes (normalized single-cell gene expression shown) per cluster. **B)** Feature Dot Plot and **C)** Feature UMAP of the marker genes used for cluster annotation. **D)** Stacked diagram showing the relative proportions of major immune cell subtypes within aged male and female *Ldlr*$^{-/-}$ aortas, measured by flow cytometry.

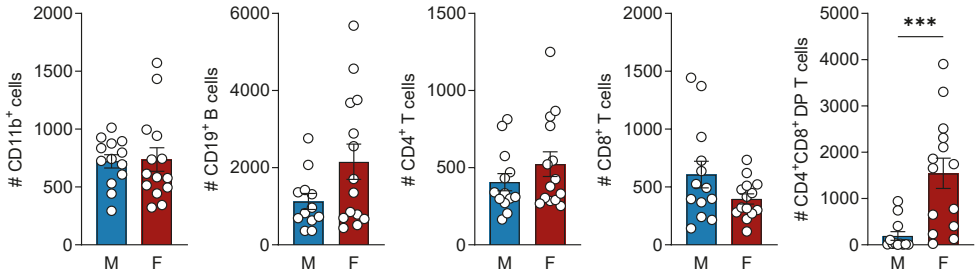


**Supplementary Figure S3. Biological distribution of immune cells in aged *Ldlr*$^{-/-}$ mice.** Flow cytometry analysis of CD11b$^{+}$ myeloid, CD19$^{+}$ B cells, CD4$^{+}$ T cells, CD8$^{+}$ T cells and double positive CD4$^{+}$ CD8$^{+}$ T cells in chow diet-fed aged male and female *Ldlr*$^{-/-}$ mice. Data are from n = 12–14 mice per group. Statistical significance was tested by a t-test. Mean ± S.E.M. plotted. ***P < 0.001.

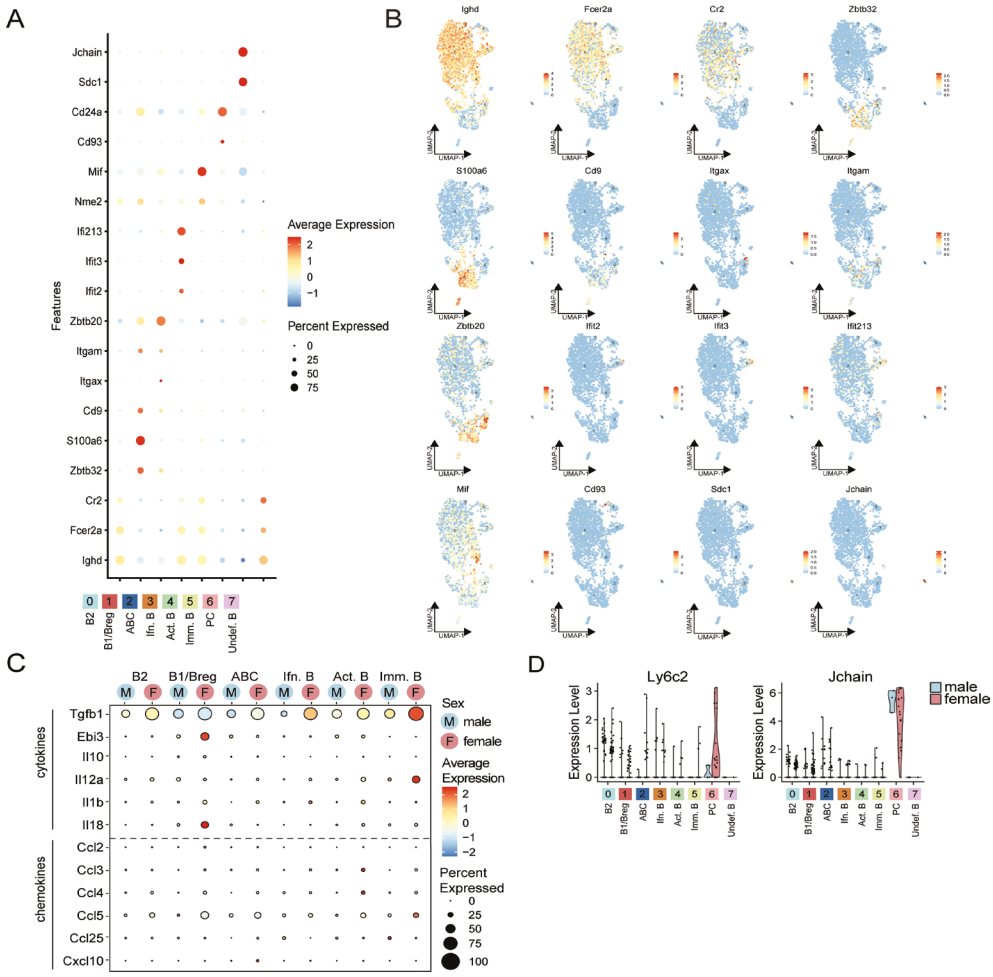


**Supplementary Figure S4. Sex-specific differences in aortic B cells of aged *Ldlr*$^{-/-}$ mice. A)** Average expression of cytokine and chemokine genes in B cell clusters split by sex. **B)** Feature Dot Plot and **C)** Feature UMAP of the marker genes used for cluster annotation. **D)** Sex-specific gene expression level of plasma cell-associated genes in B cell clusters.

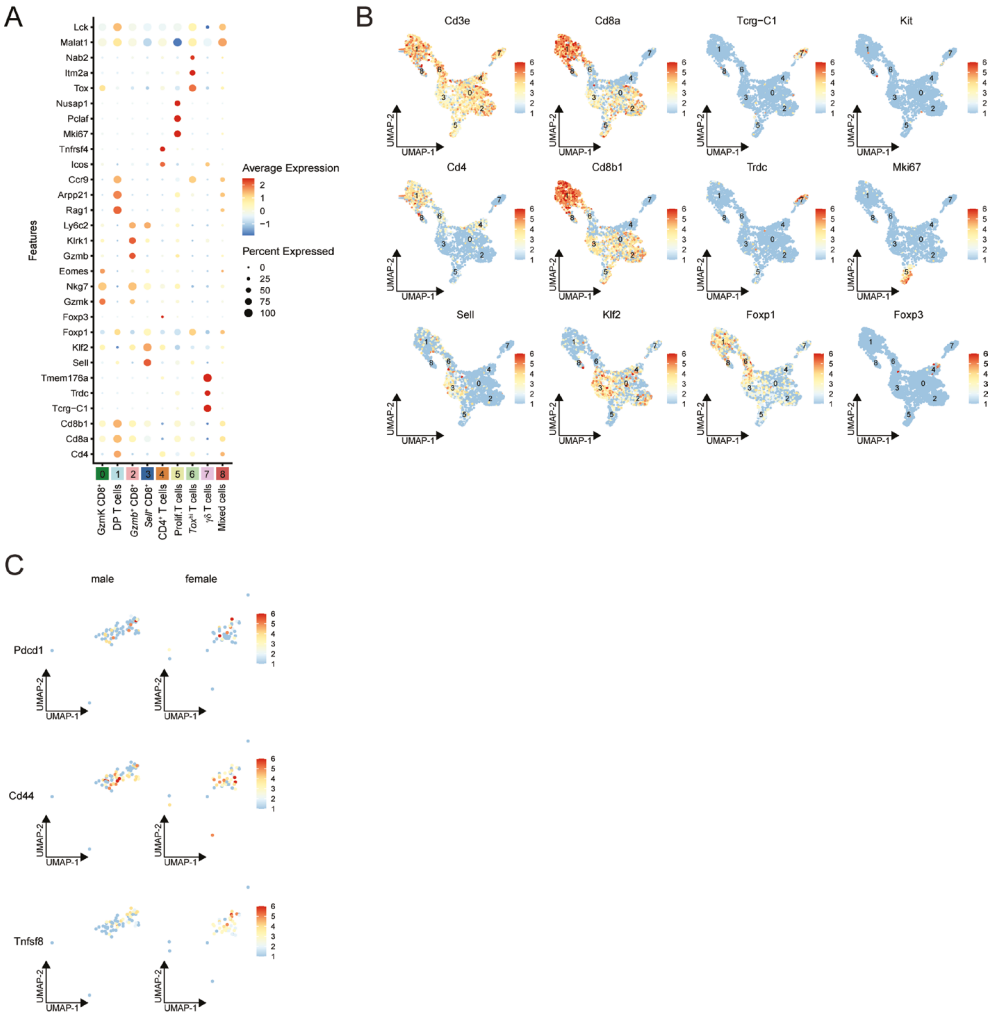


**Supplementary Figure S5. Characterization of aortic T cells in aged *Ldlr*$^{-/-}$ mice. A)** Feauture Dot Plot of the marker genes used for cluster annotation. **B)** Average expression of canonical markers in T cell clusters projected on the UMAP plot. **C)** UMAP projection displaying sex-specific expression level of genes characteristic for senescence-associated CD4$^{+}$ T cells.

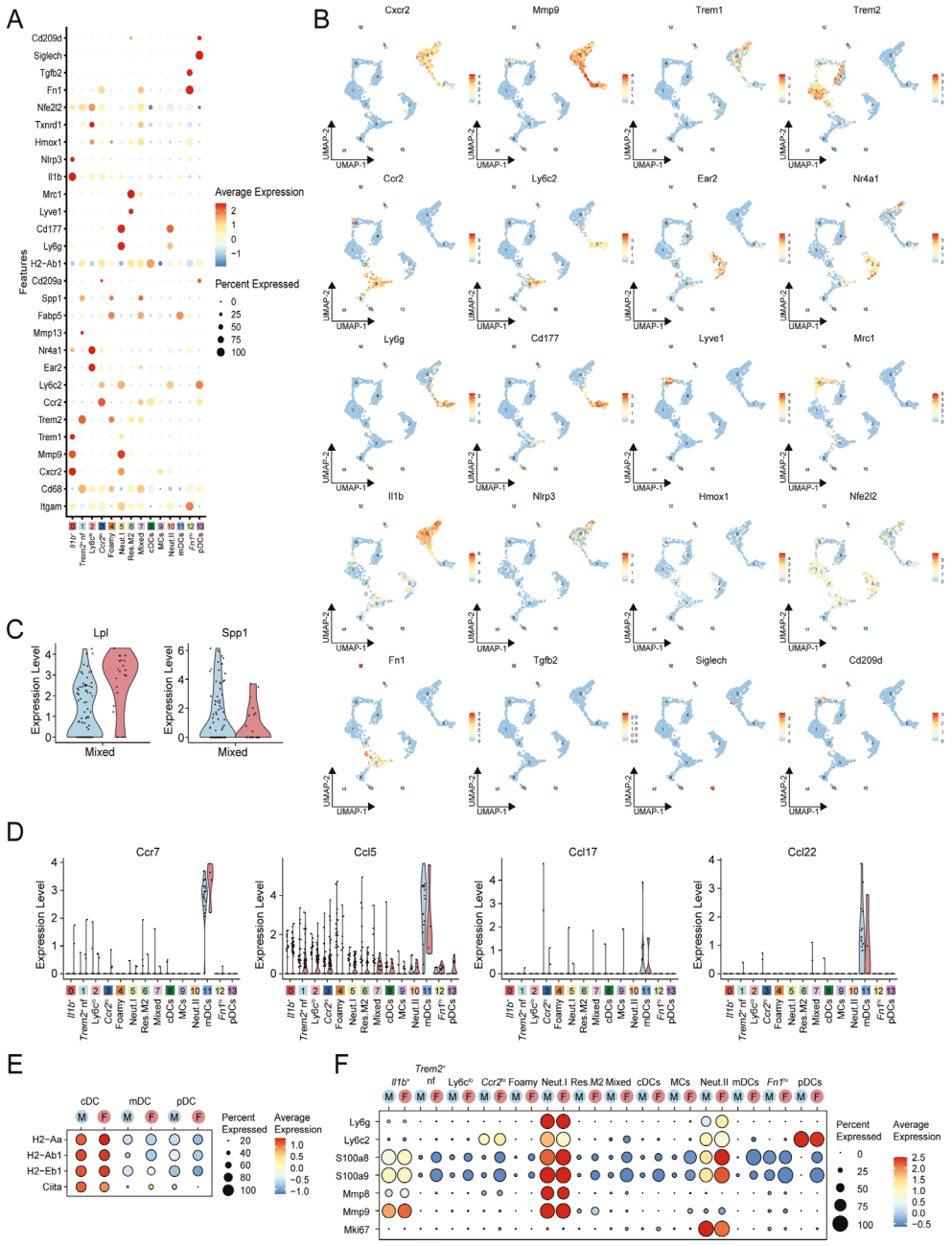


**Supplementary Figure S6. Comparison of aortic myeloid cells between aged male and female *Ldlr*$^{-/-}$ mice. A)** Feature Dot Plot and **B)** Feature UMAP of the marker genes used for cluster annotation. Sex-specific expression of **C)** differentially expressed genes in cluster 7 and **D)** chemotaxis genes specific for migratory dendritic cells. **E)** Average expression of MHCII-related genes in dendritic cell clusters split by sex. **F)** Average expression of neutrophil markers in myeloid cell clusters split by sex.

# SUPPLEMENTARY TABLES

**Supplementary Table S1. Major Resources Table**

**Antibodies (*in vivo* studies)**

| Species | Vendor or Source | Background Strain | Sex | Persistent ID / URL |
|---|---|---|---|---|
| Mouse, *Ldlr*$^{-/-}$ | Jackson | C57BL/6J | Male | www.jax.org |
| Mouse, *Ldlr*$^{-/-}$ | Jackson | C57BL/6J | Female | www.jax.org |

**Antibodies**

| Target antigen | Vendor or Source | Catalog # | Working concentration | Persistent ID / URL |
|---|---|---|---|---|
| **Mouse** | | | | |
| MOMA-2 | Bio-Rad (formerly AbD Serotec) | MCA519G | 1:1000 | www.bio-rad-antibodies.com |
| α-Rat | Vector | BA-4001 | 1:200 | www.vectorlabs.com |
| CD4 – V500 | BD Biosciences | 560782 | 1:1000 | www.bdbiosciences.com |
| CD8a – AF700 | Biolegend | 100730 | 1:500 | www.biolegend.com |
| CD19 – BV605 | Biolegend | 115540 | 1:500 | www.biolegend.com |
| CD11b – PE | eBioscience | 12-0112-82 | 1:1000 | www.thermofisher.com/ebioscience |
| CD11c – FITC | Biolegend | 117306 | 1:800 | www.biolegend.com |
| CD8a – PE-Texas Red | Invitrogen | MCD0817 | 1:1000 | www.thermofisher.com/invitrogen |
| CD45 – AF700 | Biolegend | 103128 | 1:1000 | www.biolegend.com |
| CD3 – eFluor450 | eBioscience | 48-0032-82 | 1:200 | www.thermofisher.com/ebioscience |
| CD11b – BV605 | Biolegend | 101257 | 1:500 | www.biolegend.com |
| PD-1 – PerCP.Cy5.5 | Biolegend | 109120 | 1:400 | www.biolegend.com |
| Ly6C – APC | eBioscience | 17-5932-82 | 1:500 | www.thermofisher.com/ebioscience |
| CD45 – AF700 | Biolegend | 103128 | 1:1000 | www.biolegend.com |
| Tox – PE | Miltenyi Biotec | 130-120-716 | 1:400 | www.miltenyibiotec.com |
| CD45 – PE | Biolegend | 103106 | 1:500 | www.biolegend.com |
| CD16/32 (Fc Block) | BD Biosciences | 553142 | 1:250 | www.bdbiosciences.com |
| Fixable viability dye – eFluor 450 | eBioscience | 65-0865-18 | 1:2000 | www.thermofisher.com/ebioscience |

**Other**

| Description | Source / Repository | Persistent ID / URL |
|---|---|---|
| Trichrome Stain (Masson) Kit | Sigma Aldrich | www.sigmaaldrich.com |
| Oil Red O | Sigma Aldrich | www.sigmaaldrich.com |
| Hematoxylin Solution, Mayer's | Sigma Aldrich | www.sigmaaldrich.com |
| RPMI 1640 | Gibco | www.thermofisher.com |
| Vectastain ABC kit (PK-4000) | Vector | www.vectorlabs.com |
| ImmPact NovaRed kit | Vector | www.vectorlabs.com |
| Collagenase I | Sigma Aldrich | www.sigmaaldrich.com |
| Collagenase XI | Sigma Aldrich | www.sigmaaldrich.com |
| Hyaluronidase | Sigma Aldrich | www.sigmaaldrich.com |

| | | |
|---|---|---|
| DNAse I | Sigma Aldrich | www.sigmaaldrich.com |
| Fetal Bovine Serum | Greiner Bio-One | www.gbo.com |

**Supplementary Table S2. Top 25 differentially expressed genes Main clustering**

| Main.00 | Main.01 | Main.02 | Main.03 | Main.04 | Main.05 | Main.06 | Main.07 |
|---|---|---|---|---|---|---|---|
| Ighd | Ccl5 | Rag1 | Ighm | Fn1 | C1qa | Lef1 | Il1b |
| Ebf1 | Nkg7 | Arpp21 | Mzb1 | Ifitm3 | C1qb | Itm2a | Retnlg |
| Cd79a | Ms4a4b | Dntt | Iglc2 | Ccr2 | C1qc | Tcf7 | Csf3r |
| Cd79b | AW112010 | Satb1 | Ms4a1 | Psap | Apoe | Tmsb10 | S100a8 |
| Mef2c | Ctla2a | Ccr9 | Iglc1 | Tgfbi | Pf4 | Trac | Ifitm1 |
| Ms4a1 | Ctsw | Cd8b1 | C130026I21 Rik | Ms4a6c | Ms4a7 | Satb1 | Slpi |
| Fcmr | Hcst | Endou | AC168977.1 | Ccl9 | Selenop | Cd27 | Msrb1 |
| Bank1 | Ms4a6b | Ldhb | Pkig | Lgals3 | Mrc1 | Cd28 | Cxcr2 |
| Iglc3 | H2-Q7 | Rmnd5a | Iglc3 | Plbd1 | Mafb | Cd3d | G0s2 |
| Iglc2 | Klrd1 | Tcf7 | Cd79a | Naaa | Ctsb | Cd5 | Mmp9 |
| Ly6d | Il2rb | Trbc2 | Ly6a | Mpeg1 | Trem2 | Prkcq | Hdc |
| Fcer2a | Xcl1 | Sox4 | H2-DMb2 | Gm2a | Trf | Rgs10 | Stfa2l1 |
| H2-DMb2 | Gzmk | Cd8a | Cd79b | Alox5ap | Dab2 | Tox | Hp |
| Cd74 | Gzmb | Themis | Napsa | Ifitm2 | Cd63 | Trbc2 | Ccl6 |
| H2-Ob | Cxcr6 | Ssbp2 | Tcf4 | Ctss | Lgmn | Txk | Mxd1 |
| Iglc1 | Gimap4 | Lck | Igkc | H2-DMb1 | Cxcl16 | Cd3g | Ifitm2 |
| Vpreb3 | Cd3g | Myb | Plac8 | Cst3 | Csf1r | Bcl11b | Tnfaip2 |
| Cd55 | Klrk1 | Cd4 | Fcmr | Lyz2 | Fcrls | Cd6 | Grina |
| Pax5 | Bcl2 | Arl5c | Ly6d | S100a4 | Cd14 | Ccr9 | Slc7a11 |
| Gm31243 | Gimap3 | Aqp11 | Zbtb20 | Vim | Timp2 | Cd2 | Ccr1 |
| Ralgps2 | Gm2682 | Mier1 | D10Wsu102e | Fabp5 | Lpl | Chd3 | Gsr |
| H2-Aa | Gimap7 | Bcl11b | Dnajc7 | Lyz1 | Adgre1 | Sox4 | Dusp1 |
| Tnfrsf13c | Trac | Tcf12 | Zcwpw1 | Ifi30 | Pltp | Ets1 | S100a9 |
| H2-Oa | Itgb1 | Trbc1 | Tppp3 | Plac8 | Hexb | Trbc1 | Cxcl2 |
| H2-Eb1 | Ly6c2 | Gm4258 | Crip1 | Retnla | Mmp12 | Ikzf2 | S100a11 |

| Main.08 | Main.09 | Main.10 | Main.11 | Main.12 | Main.13 | Main.14 | Main.15 |
|---|---|---|---|---|---|---|---|
| Trdc | Ear2 | Stmn1 | Cd5l | Camp | Ncr1 | Siglech | Fscn1 |
| Tmem176a | Ace | Top2a | Cd63 | Ngp | Klrb1c | Cox6a2 | Cacnb3 |
| Tmem176b | Clec4a3 | Mki67 | Gpnmb | Ltf | Klra4 | Klk1 | Ccl22 |
| Tcrg-C1 | Eno3 | Hist1h2ae | C1qb | Lcn2 | Klra8 | Gm21762 | Socs2 |
| Cd163l1 | Treml4 | Hist1h1b | C1qc | Wfdc21 | Klrb1b | Fcer1a | Zmynd15 |
| Cxcr6 | Cd300e | Pclaf | C1qa | Chil3 | Klrb1a | Gata2 | Tbc1d4 |
| Il18r1 | Csf1r | Ube2c | Fabp5 | Mmp8 | Klra9 | Cpa3 | Anxa3 |
| Actn2 | Grk3 | Hist1h3c | Trem2 | Ifitm6 | Klre1 | Smim5 | Rogdi |
| Trdv4 | Clec4a1 | Birc5 | Mmp12 | Cd177 | Klrc2 | Atp1b1 | Cxcl16 |
| Podnl1 | Adgre4 | Rrm2 | Apoe | Mmp9 | Klra7 | Cd7 | Serpinb6b |
| Kcnk1 | Dusp16 | Cenpf | Ftl1 | Ly6g | Klrk1 | Cyp11a1 | Ccr7 |
| Ltb4r1 | Cx3cr1 | Nusap1 | Ms4a7 | Adpgk | Prf1 | Plac8 | Relb |
| Ly6g5b | Lst1 | Hist1h2ap | Fth1 | Mcemp1 | Gzma | Tyrobp | Basp1 |
| Il7r | Pla2g7 | H2afx | Lgals3 | Cebpe | Serpinb9 | Csf1 | Fabp5 |
| Tmem64 | Clec4e | Dut | Wfdc17 | Mgst1 | Gzmb | Rnase6 | Gadd45b |
| Maf | Ms4a6c | Hmgn2 | Spp1 | Hp | Klrd1 | Ctsl | Tmem176a |

| | | | | | | | |
|---|---|---|---|---|---|---|---|
| Ckb | Tnfrsf1b | Anp32e | Ctsb | Retnlg | Il2rb | Tcf4 | Etv3 |
| Ramp1 | Gngt2 | Ptma | Ctsl | Anxa1 | Serpinb6b | Ifitm1 | Syngr2 |
| S100a4 | Cebpb | Hmgb1 | Cd68 | Dstn | Ctsw | Bst2 | Traf1 |
| Serpinb1a | Nr4a1 | H2afz | Serpinb6a | Pglyrp1 | Nkg7 | Hdc | Samsn1 |
| Lmo4 | Fcer1g | Hmgb2 | Ctsd | S100a8 | Cd7 | Ccl4 | Tmem123 |
| Blk | Cybb | Tuba1b | Selenop | S100a9 | AW112010 | Irf8 | Marcks |
| Emb | Sat1 | H2afv | Cstb | Prdx5 | Xcl1 | Ccl3 | Map4k4 |
| Ifngr1 | Plek | Ube2s | S100a1 | Cybb | Ccl5 | Ccl9 | Cst3 |
| Cd3g | Prdx1 | Tubb5 | Ctss | Lyz2 | Ccl4 | Ccl6 | Ifi30 |

**Supplementary Table S3. Top 25 differentially expressed genes B cell clustering**

| **B.00** | **B.01** | **B.02** | **B.03** | **B.04** | **B.05** | **B.06** | **B.07** |
|---|---|---|---|---|---|---|---|
| Ighd | S100a6 | Nt5e | Ifit3 | Srm | Akap12 | Derl3 | Fchsd2 |
| Fcer2a | Ahnak | AC168977.1 | Ifi213 | Nop58 | Atp1b1 | Fam46c | Gm20559 |
| Mef2c | Zbtb32 | AC133103.1 | Usp18 | Ncl | Fam129c | Jchain | Zfp329 |
| Satb1 | Ahnak2 | Itm2c | Ifit2 | C1qbp | Vpreb3 | Iglv1 | Chd2 |
| Neurl3 | Lmna | C130026I21 Rik | Irf7 | Nme1 | Myb | Slpi | C1qa |
| Ralgps2 | Anxa2 | Itgb1 | Slfn5 | Hsp90ab1 | Pafah1b3 | Mt1 | BE692007 |
| Stk17b | Rassf4 | Adgre1 | Ifi206 | Eif4a1 | Cd79b | Ly6c2 | Slc38a2 |
| Fchsd2 | Vim | Zbtb20 | Ifi203 | Ddx21 | Sox4 | Creld2 | Gm31243 |
| Cd55 | Tppp3 | Bhlhe41 | Zbp1 | Mif | Ly6d | Tmem176b | Cd69 |
| Cr2 | Myadm | Fgl2 | Ifi27l2a | Nhp2 | Cd24a | Prdx4 | Macf1 |
| Sell | Itgb1 | Ighg3 | Ifi214 | Gnl3 | Spib | Edem1 | Plk2 |
| H2-Ob | Pdlim1 | Zeb2 | Trim30a | Ranbp1 | Cecr2 | Xbp1 | Zfp869 |
| Pxdc1 | Lgals1 | Txn1 | Stat1 | Npm1 | Iglc1 | Sdf2l1 | Atxn2 |
| Pxk | S100a4 | H2-Q7 | Ms4a4c | Ppp1r14b | Hck | Txndc5 | Zcchc7 |
| Zfp318 | Crip1 | Tcf4 | Shisa5 | Hspe1 | Siglecg | Pdia4 | Pan2 |
| Pold4 | Tagln2 | Fcgr2b | Ifi208 | Dkc1 | Chchd10 | Igkc | Mycbp2 |
| Gm31243 | Atf3 | Lgals1 | Xaf1 | Set | Arl5c | Ighg2c | Kidins220 |
| Smad7 | Plac8 | Pld4 | Ifi209 | Eif5a | Cnp | Ssr4 | 2810013P06 Rik |
| Icosl | Ccnd2 | Apoe | Ifi47 | Fbl | Dnajc7 | Sec11c | Slc12a6 |
| Gm8369 | S100a11 | Ptpn1 | Rnf213 | Hspd1 | Tifa | Hsp90b1 | Usp15 |
| Bmyc | S100a10 | Igha | Parp14 | Pa2g4 | Tcf3 | Manf | Txndc16 |
| Dmxl1 | Zcwpw1 | Tnfaip8 | Phf11b | Psme2 | Bcl7a | Mzb1 | Akap9 |
| Lmo2 | Cd2 | Fcer1g | Samhd1 | Hspa5 | Rgs2 | Slc3a2 | Tut7 |
| H2-Eb2 | Zbtb20 | Cd72 | Bst2 | Il4i1 | Marcks | Ighg1 | Arid1a |
| Tecpr1 | D10Wsu102e | Xist | Tor3a | Ccnd2 | Ifi30 | Ighg2b | Cxcr4 |

**Supplementary Table S4. Top 25 differentially expressed genes T cell clustering**

| **T.00** | **T.01** | **T.02** | **T.03** | **T.04** | **T.05** | **T.06** | **T.07** | **T.08** |
|---|---|---|---|---|---|---|---|---|
| Gzmk | Rag1 | Gzmb | Sell | Tnfrsf4 | Pclaf | Itm2a | Tmem176a | Malat1 |
| Nkg7 | Arpp21 | Klrk1 | Rps20 | Gpm6b | Hist1h3c | Rgs10 | Tmem176b | Lck |
| Ctla2a | Dntt | Itga1 | Rps19 | Izumo1r | Rrm2 | Lef1 | Tcrg-C1 | Prrc2c |
| Ccl5 | Endou | Klrd1 | Ccr7 | Maf | Birc5 | Satb1 | Serpinb1a | Ptprc |
| Ms4a4b | Rmnd5a | Ccl5 | Rpl23 | Ifi27l2a | Nusap1 | Sox4 | Blk | Mbnl1 |
| Eomes | Ldhb | Nkg7 | Rps16 | Ly6a | Cenpf | Tox | Actn2 | mt-Nd4 |
| Hcst | Ccr9 | Ly6c2 | Rplp1 | Capg | Mki67 | Gsn | Pxdc1 | mt-Cytb |

| | | | | | | | | |
|---|---|---|---|---|---|---|---|---|
| AW112010 | Aqp11 | AW112010 | Rpl13 | Icos | Hist1h2ab | Ccr9 | Kcnk1 | Ccr9 |
| Rpl13a | Myb | Fgl2 | Rps28 | Tnfsf8 | Ube2c | Cnn3 | Ltb4r1 | Mier1 |
| Itga4 | Satb1 | Ctsw | Rps24 | Tnfrsf18 | Lig1 | Tmsb10 | Trdv4 | Arpp21 |
| H2-K1 | Ssbp2 | Lgals3 | Rps7 | Pou2f2 | Top2a | Basp1 | Cd163l1 | Ets1 |
| Rgs1 | Arl5c | Zeb2 | Rps18 | Shisa5 | Stmn1 | Cd28 | Ckb | Srrm2 |
| H2-Q7 | Sox4 | Ahnak | Dapl1 | Hif1a | Dut | Cd2 | Podnl1 | Tnrc6b |
| Ccr5 | Cd4 | Itgb1 | Ms4a4c | Eea1 | Hist1h2ae | Id3 | Igf1r | Cd164 |
| Ms4a6b | Dgkeos | Cx3cr1 | Rpl36a | Nrp1 | Tuba1b | Ikzf1 | Capg | Son |
| Pdcd1 | Mier1 | Klre1 | Rpl12 | Cd82 | Hmgn2 | Cd5 | Maf | Akap13 |
| Tox | Ets2 | Gzma | Rpl39 | Ctla4 | Ptma | Ikzf2 | Trdc | Clk1 |
| Gimap7 | Tcf7 | Klrc1 | Rps12 | Tbc1d4 | Hist1h1b | Cd27 | Il18r1 | Thrap3 |
| Bcl2 | Themis | Cd226 | Rps5 | S100a11 | H2afx | Hivep3 | Selenop | Ppp2ca |
| Gm8369 | Gtf2h4 | Id2 | Eef1b2 | Ltb | Ran | Xist | Ccr2 | Kpna4 |
| Ccl4 | Xrcc6 | S100a6 | S1pr1 | Srgn | Hist1h2ap | Etnk1 | Lmo4 | Selenos |
| Zfp36l2 | Tcf12 | Lgals1 | Klf2 | Odc1 | Hmgb2 | Cytip | S100a4 | Itgb1 |
| Runx3 | Cyb5a | Cd48 | Igfbp4 | Junb | H2afz | Sept7 | Il7r | Lyz2 |
| BE692007 | Ly6d | Ccl4 | Ly6c2 | Ikzf2 | Tubb5 | Egr1 | Cxcr6 | Tnrc6c |
| Cst7 | Gm4258 | Xcl1 | Gzmm | Samhd1 | Hist1h4d | Trbc1 | S100a6 | Wbp11 |



**Supplementary Table S5. Top 25 differentially expressed genes myeloid cell clustering**

| My.00 | My.01 | My.02 | My.03 | My.04 | My.05 | My.06 |
|---|---|---|---|---|---|---|
| Cxcr2 | Nes | Cd300e | Ms4a4c | Cd5l | Itgb2l | Cbr2 |
| Csf3r | Cd72 | Treml4 | Ccr2 | Ftl1 | Ly6g | Mgl2 |
| Hdc | Cadm1 | Ace | Vcan | Fth1 | Cd177 | Cd163 |
| Il1b | Ms4a7 | Eno3 | S100a4 | Atp6v0d2 | Ngp | Mrc1 |
| H2-Q10 | Myo1e | Adgre4 | Fn1 | Fabp5 | Ltf | Lyve1 |
| Mmp9 | Zmynd15 | Ear2 | Plac8 | Lgals3 | Wfdc21 | Igfbp4 |
| Mxd1 | Cxcl16 | Spn | Ms4a6c | Gpnmb | Adpgk | Gas6 |
| Msrb1 | C3ar1 | Dusp16 | Tmsb10 | Apoe | Chil1 | Pf4 |
| Junb | Trem2 | Pou2f2 | Itgb7 | Syngr1 | Lcn2 | C4b |
| Slpi | Igf1 | Grk3 | Ms4a6b | Cd63 | Camp | Folr2 |
| Dusp1 | Slamf9 | Gngt2 | Ifitm3 | Mmp12 | Cebpe | Stab1 |
| Ccr1 | Mafb | Nr4a1 | Napsa | Trem2 | Ckap4 | Maf |
| Srgn | C1qa | Itgal | Slfn5 | Serpinb6a | Ly6c2 | F13a1 |
| S100a11 | C1qc | Itga4 | Ly6c2 | Lgals1 | Mmp8 | Fcrls |
| Fgl2 | Hexb | Myo1g | H2-DMa | Cstb | Serpinb1a | Cd209f |
| Sell | Gatm | Cybb | H2afy | Ctsd | Ifitm6 | Dab2 |
| Ifitm1 | C1qb | Clec4a3 | Ifi209 | Ctsl | S100a8 | Ccl8 |
| Grina | Mmp12 | Clec4a1 | Ahnak | Wfdc17 | S100a9 | Ccl12 |
| Slc7a11 | Clic4 | Stap1 | S100a10 | Igf1 | Pglyrp1 | Tmem176b |
| Il1r2 | Anxa5 | Tnfrsf1b | Crip1 | Spp1 | Syne1 | Cfh |
| Lrg1 | Lmna | Bcl2a1d | Vim | Il18bp | Mmp9 | Selenop |
| Stfa2l1 | Lpl | Ms4a6c | Ifi27l2a | Pld3 | Anxa1 | Fcgrt |
| Ptgs2 | Rgs1 | Apoc2 | Lyz2 | AY036118 | Chil3 | Ctsc |
| G0s2 | Ctsb | Txnrd1 | Ifi30 | Ftl1-ps1 | Retnlg | Trf |
| Cxcl2 | Apoe | Prdx1 | Thbs1 | S100a1 | Hmgn2 | Ccl7 |

| My.07 | My.08 | My.09 | My.10 | My.11 | My.12 | My.13 |
|---|---|---|---|---|---|---|
| Emp1 | Xcr1 | Gata2 | Birc5 | Cacnb3 | Tgfb2 | Gm21762 |
| S100a10 | Sept3 | Cpa3 | Hist1h3c | Fscn1 | Ltbp1 | Klk1 |
| Fn1 | Itgae | Csrp3 | Fcnb | Ccr7 | Prg4 | Atp1b1 |
| Psap | Ifi205 | Fcer1a | Pclaf | Ccl22 | Ptgis | Cox6a2 |
| Capg | Olfm1 | Ms4a2 | Ube2c | Socs2 | Alox15 | Siglech |
| F10 | Wdfy4 | Cyp11a1 | Mki67 | Serpinb6b | Selp | Upb1 |
| Apoc2 | Naaa | Cd200r3 | Top2a | Apol7c | Ednrb | Spib |
| Cstb | Naga | Sytl3 | Elane | Serpinb9 | Saa3 | Ccr9 |
| Lgals3 | Irf8 | Mcpt8 | Cebpe | Tbc1d4 | Fcna | Iglc3 |
| Gpnmb | Plbd1 | Il6 | Hist1h1b | Clu | Serpinb2 | Cd7 |
| Plin2 | Psmb9 | Nedd4 | Hist1h2ae | Il4i1 | Icam2 | Smim5 |
| Ctss | Cst3 | Cd7 | Stmn1 | Relb | Flnb | Bcl11a |
| Ifi30 | Gng10 | Ctsg | Serpinb1a | Zmynd15 | C4b | Rpgrip1 |
| Lgals1 | H2-DMb1 | Il18r1 | Ltf | Traf1 | Ltc4s | Ly6d |
| Ahnak | Ckb | Cd69 | Camp | Birc2 | Ecm1 | Runx2 |
| Atp6v0c | H2-DMa | Csf1 | Hist1h2ap | Ccl5 | Fn1 | Fyn |
| Lgmn | Ppt1 | Ifitm1 | Ngp | Tmem123 | Fabp4 | Rnase6 |
| Lpl | Psmb8 | Ccl4 | Chil3 | Anxa3 | Itga6 | Ly6a |
| Ccl9 | Eef1b2 | Ets1 | Prtn3 | Etv3 | Cxcl13 | Tcf4 |
| Fabp5 | H2-Ab1 | Serpinb1a | Hmgn2 | Syngr2 | Cfp | Dnajc7 |
| Prdx1 | H2-Eb1 | Jun | Wfdc21 | Map4k4 | Fam46a | Bst2 |
| Clec4n | Id2 | Tmem71 | Lcn2 | Tmem176a | Emilin2 | Irf8 |
| Spp1 | H2-Aa | Ccl3 | Hmgb2 | AW112010 | Pycard | Ly6c2 |
| Retnla | Tmsb10 | Rgs1 | H2afz | Fabp5 | Tagln2 | Plac8 |
| Lyz1 | Cd74 | Ccl9 | S100a8 | Epsti1 | Slpi | Xist |

# 4